SU-SEL-65-092

Lattice Vibration Spectra of $GaAs_xP_{1-x}$ Single Crystals

by

Yen-sun Chen

October 1965

Technical Report No. 5108-1

Prepared under
National Aeronautics and Space Administration
Research Grant No. NsG-555

SOLID-STATE ELECTRONICS LABORATORY

STANFORD ELECTRONICS LABORATORIES

STANFORD UNIVERSITY • STANFORD, CALIFORNIA

Requests for copies of this report should be referred to:

National Aeronautics and Space Administration
Office of Scientific and Technical Information
Washington, D.C. 20546
Attn: AFSS-A

SEL-65-092

LATTICE VIBRATION SPECTRA OF $GaAs_xP_{1-x}$ SINGLE CRYSTALS

by

Yen-sun Chen

October 1965

Technical Report No. 5108-1

Prepared under
National Aeronautics and Space Administration
Research Grant No. NsG-555

Solid-State Electronics Laboratory
Stanford Electronics Laboratories
Stanford University Stanford, California

ABSTRACT

1916?

Single crystals of $GaAs_xP_{1-x}$ were successfully grown in an open-tube epitaxial vapor growth system. Interactions of photons with phonons in the alloy crystals were investigated by means of reflectivity and transmission measurements in the infrared spectral region.

Crystals were grown in an H_2 atmosphere on GaAs seeds, using PCl_3, $AsCl_3$, and Ga as source materials. These crystals were found to be low in carrier concentration, consistently below 10^{15} cm^{-3} (electrons) at room temperature, and to be free of any gross inhomogeneity in the distribution of constituent atoms.

Reflectivity spectra of $GaAs_xP_{1-x}$ were taken at 300 ^oK in the spectral region of 220 to 500 cm^{-1}. Two Reststrahlen modes whose frequencies were close to those of TO(Γ) phonons in GaAs and GaP, respectively, were detected in the alloy. The absence of the GaAs-like mode in the GaP-rich samples is in good agreement with the theory given by Dawber and Elliott. Absorption spectra in $GaAs_xP_{1-x}$ were taken at 300 ^oK in the region of 400 to 800 cm^{-1}. A superposition of the two-phonon bands characteristic of GaAs and GaP was observed in the alloy. The energies of several GaAs and GaP phonons in the alloy were calculated, based on Johnson's assignment schemes, as a function of composition. An absorption band, which is identified as the "summation" band of the two TO(Γ) phonons in the alloy, was found near 610 cm^{-1} in the GaAs-rich samples. The existence of such a band suggests that interaction between As and P atoms in the lattice is significant.

The superposition of bands characteristic of GaAs and GaP in the two-phonon absorption spectra of the alloys is attributed to the presence of microscopic clustering of the minority constituent associated with the random atomic distribution. The Reststrahlen band spectra of these alloys are explained by a model in which the presence of two resonant modes is attributed mainly to the vibration of As and P atoms against Ga atoms in the lattice as the first nearest neighbors. The frequency shifts of these modes in the alloy are fitted by a parameter representing the interaction between As and P atoms as second nearest neighbors.

authors

This is a virtual crystal model in that average parabolic potentials are given to the three species of atoms in the lattice. Good agreement is obtained between the data and the theoretical calculations. The model thus demonstrates that it is incorrect to interpret the results in this work by the assumption of gross inhomogeneity in the distribution of constituent atoms in the alloy.

CONTENTS

CONTENTS (CONT)

TABLES

ILLUSTRATIONS

SYMBOLS

c	speed of light
$\vec{d}_j$	polarization vector of photon
e	electron charge
$\vec{f}$	polarization vector of phonon
h	Planck's constant
$\hbar$	$h/2\pi$
k	Boltzmann's constant (used in the thermal energy kT)
k	extinction coefficient
$\vec{k}$	crystal momentum and wave vector of phonon
$\vec{k}_j$	wave vector of phonon of the j^{th} branch
$\vec{k}_o$	wave vector of photon
$\vec{k}_{TO}$	wave vector of $TO(\Gamma)$ phonon
m	mass
n	index of refraction
$\bar{n}$	complex index of refraction
$n(\vec{k}_j)$	occupation number of phonon of the j^{th} branch
n_o	electron concentration
r	ratio of flow rates
t	time
$u, \dot{u}, \ddot{u}$	atomic displacement and its first and second derivatives with respect to time
w	relative atomic displacement
x	mole fraction of As in the alloy
C_V	specific heat per gram atom at constant volume
C_{Vj}	C_V of the j^{th} phonon mode
$\vec{E}$	electric field vector

SYMBOLS (Cont)

E_{loc}	crystal local field
E_L	longitudinal polarization field
F, F_o	force constant and its value at $x = 0$
$\vec{H}$	magnetic field vector
K	compressibility
$K\alpha_1$, $K\alpha_2$	wavelength of characteristic X-ray radiation
L	$(\frac{1}{2},\frac{1}{2},\frac{1}{2})$ point in the Brillouin zone
LA	longitudinal acoustical phonon
LO	longitudinal optical phonon
M_R	reduced mass
P	polarization
P_L	longitudinal polarization
R	reflectivity
T	temperature
TA	transverse acoustical phonon
TO	transverse optical phonon
V, ΔV	volume of one gram atom and its incremental change
W	$(1,\frac{1}{2},0)$ point in the Brillouin zone
X	$(1,0,0)$ point in the Brillouin zone
$\mathcal{E}_g$	energy gap
$\mathcal{E}_p$	phonon energy
ℓ	thickness of sample
$\mathcal{T}$	transmittance

SYMBOLS (Cont)

α	absorption coefficient
β	force constant
γ	damping constant
γ_{Gr}, γ_j	Grüneisen constant and its value of the j^{th} phonon mode
$\bar{\epsilon}(\omega)$	complex dielectric constant
ϵ_o	static dielectric constant
ϵ_∞	high-frequency dielectric constant
ζ, ζ_o	force constant of Ga-As bonds and its value at $x = 0$
η, η_o	force constant of As-P bonds and its value at $x = 0$
θ	$[d(F/F_o)/dx]$
θ_B	Bragg angle
λ	wavelength
μ, μ_{vac}	permeability and its value in vacuum
ν	frequency
ξ, ξ_o	force constant of Ga-P bonds and its value at $x = 0$
σ	conductivity
ω	$2\pi\nu$
ω_j	frequency of phonon of the j^{th} branch
ω_o	frequency of photon
ω_0	resonant frequency
ω_{LO}	frequency of LO(Γ) phonon
ω_p, $\Delta\omega_p$	phonon frequency and its incremental change
ω_{TO}	frequency of TO(Γ) phonon
Ω	volume per molecule

ACKNOWLEDGMENT

The author wishes to thank his advisors, Professors G. L. Pearson, W. E. Spicer, and J. L. Moll for their constant guidance and encouragement throughout the course of this study. He is also greatly indebted to Professors W. Shockley and J. W. Allen of Stanford, Dr. Frank Herman of the Lockheed Missiles & Space Company Research Laboratory in Palo Alto, and Professor W. G. Spitzer of the University of Southern California for their many helpful suggestions. Thanks are due Professor A. L. Schawlow of Stanford and Professor Spitzer for the use of spectrometers in their laboratories.

I. INTRODUCTION

The determination of the vibrational spectra of disordered systems is a problem of considerable current interest and is one that has attracted many workers in the past few years. Dean [Ref. 1] applied mathematical techniques to obtain quantitatively accurate results for the spectra of disordered diatomic chains. However, a complete theory of three-dimensional disordered systems is yet to be developed. The alternative approach is to study such systems by the experimental method. Results of this nature were reported by Oswald [Ref. 2] on the infrared lattice absorption spectra of $InAs_xP_{1-x}$, and by Braunstein [Ref. 3] on Si-Ge alloys. The former gave only a brief survey of the problem which was carried out in a narrow region of the radiation spectra. The latter gave a detailed analysis of the spectra. Characteristics of Si- and Ge-phonon bands were found in the lattice absorption spectra of the alloy; such a phenomenon was attributed by Braunstein to the presence of Si and Ge aggregates in the material. Unfortunately, the first-order photon-phonon interaction cannot be observed in the Si-Ge alloys due to the homopolar nature of the material. It is clear that more experimental work is needed in this field.

In the present work the interactions of infrared radiation with phonons in the $GaAs_xP_{1-x}$ alloy system are investigated. This particular alloy system was chosen for three reasons:

1. Macroscopically homogeneous crystals can be grown by the epitaxial vapor deposition method,
2. A strong first-order photon-phonon interaction exists in addition to the weak higher order interactions, and
3. A great deal of interest has been shown in the system's numerous applications, such as light sources, injection lasers, and the recently discovered microwave oscillators.

The main purpose of the research described in this report is twofold:

1. To determine the effect of the disorder on the two-phonon absorption bands in the alloy, and
2. To investigate the behavior of the Reststrahlen bands as a function of alloy composition.

These studies are essential in order to obtain the fundamental knowledge of phonon spectra in disordered systems.

One of the important contributions of this work is the development of a process for growing single crystals of $GaAs_xP_{1-x}$. An open-tube epitaxial vapor growth system employing halide transport is used. The process and the properties of crystals are given in Chapter II. A brief review is given in Chapter III of the existing theories relating to the single-phonon (first order) and the two-phonon (second order) interactions with infrared radiation. The experimental results are given in Chapters IV and V: the former is concerned with the Reststrahlen bands in $GaAs_xP_{1-x}$ (single-phonon interaction) and the latter is concerned with the two-phonon absorption bands in $GaAs_xP_{1-x}$. The findings in both types of experiments are similar in that the measured spectra give a superposition of the bands characteristic of GaAs and GaP. The interpretation of these spectra is given in Chapter VI. The phenomenon of superposition can be explained without the assumption of gross inhomogeneity in the distribution of the constituent atoms; such inhonogeneity is known to be absent in these crystals. In particular, the spectra of the Reststrahlen bands in the alloy can be explained by a virtual crystal model in which average parabolic potentials are given to the three species of atoms in the lattice. Quantitative calculations based on this model give results in good agreement with the observed data. Chapter VII summarizes the results of the present work as a whole.

II. CRYSTAL GROWTH

An open-tube epitaxial vapor growth system was employed to grow single crystals of $GaAs_xP_{1-x}$. Alloys with x ranging from 0 to 1 were successfully grown with excellent reproducibility. Carrier concentration at room temperature was consistently low, of the order of 10^{15} cm^{-3} or less. These crystals were exceedingly homogeneous in compositions, less than ± 0.0025 in Δx. The thickness of the epitaxial layer was typically 0.5 mm with an area of 1 cm^2.

A. DESCRIPTION OF THE SYSTEM

The system was initially developed by Gibbons and Prehn [Ref. 4], and a detailed description of the equipment is given in their report. The system was further developed by the author to grow $GaAs_xP_{1-x}$ single crystals with properties appropriate for this study. A sketch of the system is shown in Fig. 1. Argon or purified hydrogen gas is fed into

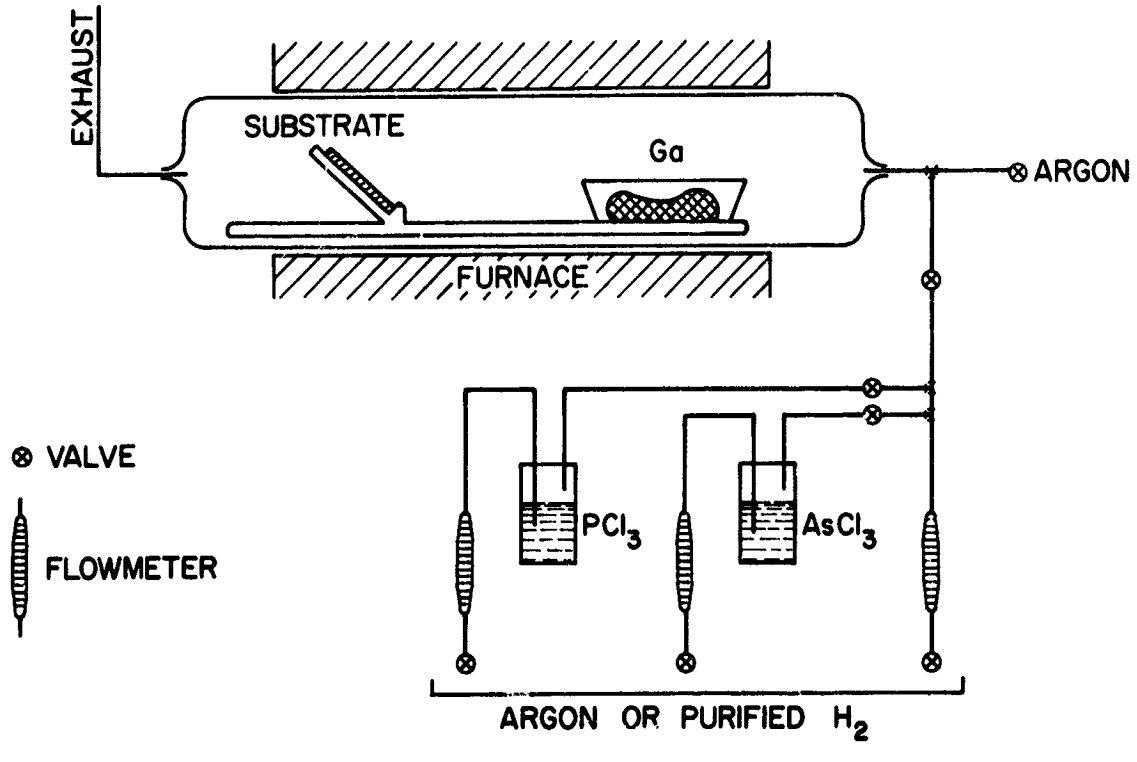

35251

FIG. 1. A SKETCH OF THE $GaAs_xP_{1-x}$ EPITAXIAL DEPOSITION SYSTEM.

the 1-in.-inside-diameter quartz reaction tube via three separate metered lines which can be adjusted to give flow rates of 0 to 100 cc/min. Two of these lines include bubblers which contain PCl_3 and $AsCl_3$ respectively; a third line provides the bypassing gas which is used to dilute the halide content as well as to obtain the desired total gas flow. A high-temperature Marshall furnace with external resistance shunts is used to obtain an appropriate temperature profile. A carrier boat is inserted inside the reaction tube with the Ga source placed at one end and the substrate at the other. And finally, the exhaust gas is burned off at the exit.

During growth, hydrogen is fed through the system together with the halides. The chemical reactions are as follows:

$$\left.\begin{array}{lr} \text{At } T \cong 1000\ ^{\circ}\text{C}, & 4PCl_3 + 12Ga \longrightarrow 12GaCl + P_4 \\ \text{At } T \cong 800\ ^{\circ}\text{C}, & 2GaCl + H_2 \longrightarrow 2HCl + 2Ga \\ & 4Ga + P_4 \longrightarrow 4GaP \\ \text{At } T < 600\ ^{\circ}\text{C}, & 3GaCl \longrightarrow GaCl_3 + 2Ga \end{array}\right\} . \qquad (2.1)$$

The same type of equation applies to the reaction involving $AsCl_3$. Notice the byproducts of this process are $GaCl_3$ and excess Ga at the cold end of the reaction tube.

An auxiliary argon line was added at the reaction tube entrance to provide a large flow of inert gas when the carrier boat is being pushed into or withdrawn from the furnace, thus avoiding contamination of both substrate and Ga from the atmosphere. During a long-growth run, $GaCl_3$ continues to deposit in the cold end of the reaction tube. To avoid clogging the exhaust path of gas flow by this deposition, which would result in poor and slow growth, it was found necessary to keep the exit end of the reaction tube free of any obstacles at the start of the growth run. Installation of this auxiliary argon line had the additional advantage of a major simplification to the system used by Gibbons and Prehn [Ref. 4] in that complicated mechanical parts--at the exit end of

the reaction tube--were no longer needed for loading and unloading the carrier boat under hydrogen atmosphere.

The second major modification to the system was the design of a new quartz carrier boat, shown in Fig. 2. The substrate was backed by a plate inclined at an angle of approximately 30 deg from the gas flow. It was found that neither laying the substrate flat nor standing it upright was satisfactory; both arrangements gave epitaxial layers with wedge-shaped cross sections, which were inconvenient as well as uneconomical for preparing samples with parallel polished surfaces as required for optical studies.

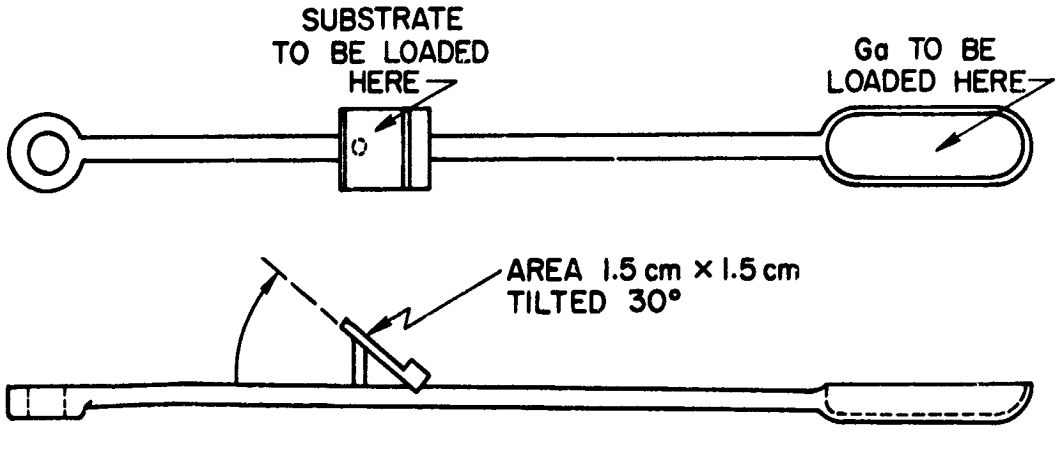

35248

FIG. 2. QUARTZ CARRIER BOAT USED IN CRYSTAL GROWTH.

B. GROWTH PREPARATIONS AND PROCEDURES

The reaction tube and the boat were cleaned in aqua regia for a few hours and then rinsed in distilled water and methanol. Because of the large difference in the thermal expansion coefficients of quartz and $GaAs_xP_{1-x}$, it was necessary to coat both the boat and the tube with carbon at the region of growth to avoid cracking of the quartz during the cooling stage as well as to ensure easy removal of residual material deposited on the boat. The coating on the inside of the tube was obtained by thermal decomposition of methane gas at 1000 ^{o}C, and the boat was smoked with carbon by holding it over a Bunsen burner.

The bubblers and other glassware were cleaned successively in HCl, distilled water, and methanol. Before filling the bubblers with PCl_3 and $AsCl_3$, precautions were taken to remove all the residual methanol to prevent reaction with the halides. The halides used in the process were reagent grade materials purchased from Baker and Adamson.*

Gallium of seven 9's purity, obtained from the Eagle-Picher Company,** was used exclusively. The metallic gallium as received was first loaded into a small quartz boat and etched in hot (60 °C) HCl to remove all Ga_2O_3 from the surface, and then rinsed in distilled water and methanol. The boat, together with the cleaned gallium, was stored under methanol until ready for use. The substrates were slices of boat-grown GaAs obtained from the Monsanto Chemical Company.*** These slices were oriented to have (111) surfaces. The (111)A and (111)B surfaces were identified by observing the shape of the etch pits following a 3-min etch in a solution of 1 part HF, 1 part H_2O_2, and 2 to 4 parts of H_2O [Ref. 5]. The etch pits on the (111)B surface are triangle shaped. For substrate preparation, the slices were cut to approximately 1 cm^2 in size, lapped with #3200 grit abrasive, etched (in a solution of 9 parts HNO_3, 1 part HF, and 10 parts H_2O) for 2 minutes and then rinsed in distilled water and methanol. The slices were then stored under methanol until ready for use.

After the furnace was heated to the proper temperature, the bubblers were filled with halides and installed into the system together with proper temperature baths; they were subsequently purged with argon gas. The reaction tube was also purged with argon to preserve the carbon coating. With the auxiliary line of argon wide open, the gallium boat and the substrate were loaded onto the carrier boat, which was placed at the entrance of the reaction tube and then quickly pushed into position in the furnace. All the argon lines were shut at this moment, and

---

*Baker and Adamson Chemical Company, Phillipsburg, N.J.

**Eagle-Picher Company, Cincinnati, Ohio.

***Monsanto Chemical Company, St. Louis, Missouri.

purified hydrogen was directed into the system. Three flowmeters shown in Fig. 1 were then carefully adjusted to the desired flow rates. The exhaust gas was burned off at the exit.

After the predetermined growth time, the furnace was turned off, the bubblers were shut off, and argon gas was used to drive out all the residual hydrogen from the reaction tube. The carrier boat was then pulled slowly from the hot zone of the furnace under a heavy argon flow from the auxiliary argon line.

C. GROWTH CONDITIONS AND RESULTS

1. Temperature Profile

The Marshall furnace was adjusted with external shunt resistors to provide the temperature profile shown in Fig. 3. The gallium boat was located at 950 °C with zero temperature gradient, and the substrate was located in the region ranging from 800 to 825 °C with a temperature gradient of 16 °C/cm.

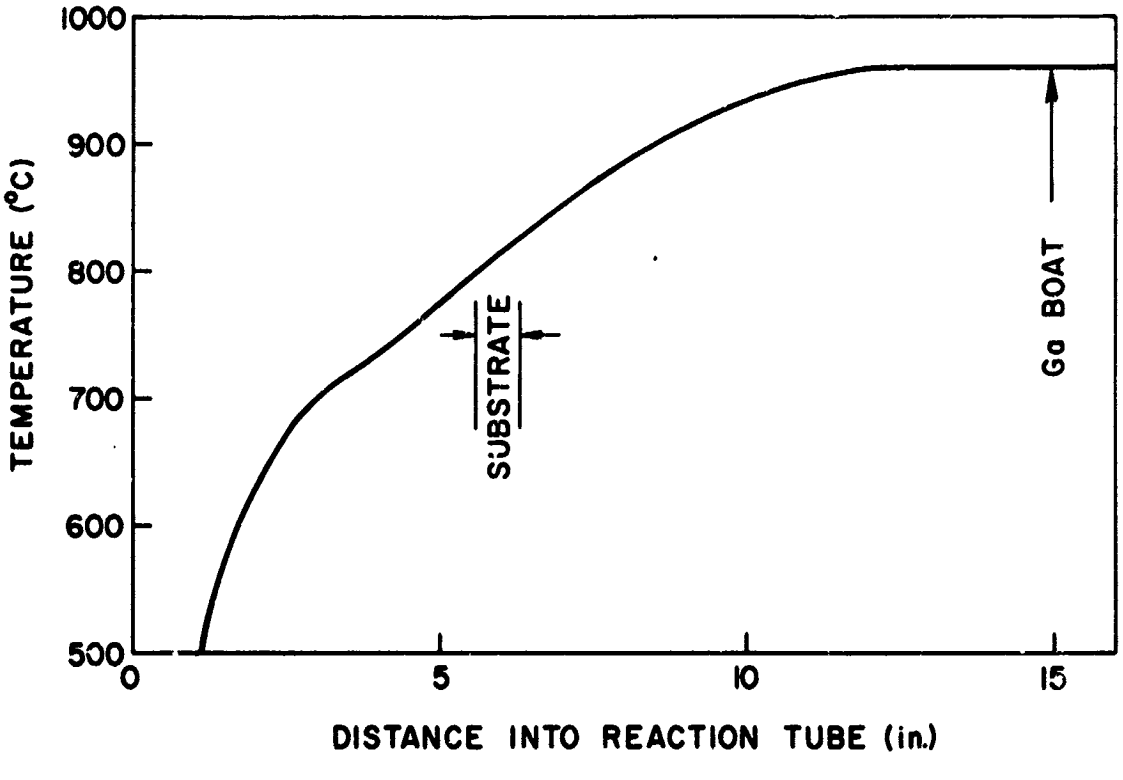

FIG. 3. TEMPERATURE PROFILE OF THE FURNACE.

2. Calculated Composition

Figure 4 gives the vapor pressure of PCl_3 and $AsCl_3$ vs temperature [Ref. 6]. It is noticed that, at a given temperature, PCl_3 has a vapor pressure ten times larger than that of $AsCl_3$. It was found necessary to operate the former at a lower temperature for good flexibility in control; 0 and 25 ^{o}C were chosen to be the temperatures of the baths for the two halides. At these temperatures, the vapor pressure of PCl_3 is 34 mm of Hg and that of $AsCl_3$ is 10.4 mm of Hg. By assuming that the hydrogen gas carries with it the saturated amount of halides in vapor form, these vapor pressures correspond to the transport of 1.98×10^{-6} and 0.56×10^{-6} moles of halide per cc of H_2 respectively. The calculated composition of arsenic, based solely on the ratio of the flow rates through the halides, is given as follows:

$$x = \frac{1}{1 + 0.283\ r} \quad , \tag{2.2}$$

where r is the ratio of the flow rate through the $AsCl_3$ bubbler (at 25 ^{o}C) to that through the PCl_3 bubbler (at 0 ^{o}C).

3. Growth Results

A total of 29 separate crystal deposits was made during this investigation. The earlier runs were made to obtain the proper temperature profile; to achieve the optimum flow rates of H_2 through the halides, as well as the total flow rate; to study the dependence of the growth rate on the crystal orientations; and to optimize other growth conditions. The results of the final eight runs, which are summarized in Table 1, are discussed in detail below.

a. The calculated composition is based on Eq. (2.2). The true composition was determined from X-ray diffraction data and Vegard's law [Ref. 7]. Figure 5 gives the relation between the calculated and the experimentally determined compositions. It is seen that, at the low phosphorous concentration end, the deviation from the calculation is large; this is believed to be caused by the diffusion of PCl_3 vapor into the system at low flow rates. This problem was solved by using a

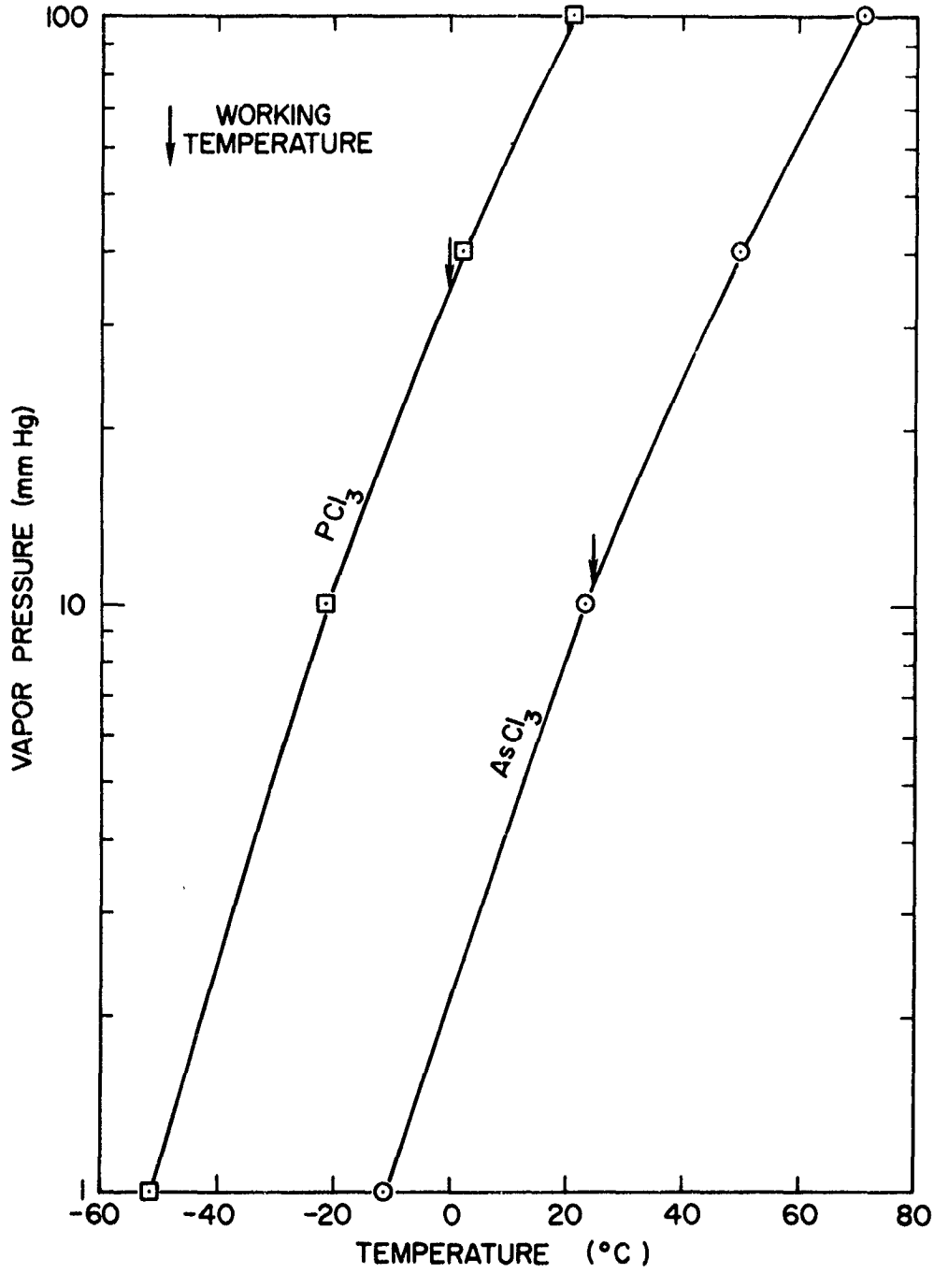

35253

FIG. 4. VAPOR PRESSURE OF $AsCl_3$ AND PCl_3 VS TEMPERATURE.

TABLE 1. CRYSTAL GROWTH DATA

Run Number	19	20	21	23	24	25	28	29
Substrate (GaAs):								
*Temperature (°C)	820	820	820	805	805	805	805	805
Orientation	(111) $(\overline{111})$	(111) $(\overline{111})$	(111)	(111)	(111)	(111)	(111)	(111)
Angle against flow (deg)	0	0	30	30	30	30	30	30
Flow of H_2 (cc/min):								
Bypass	54	54	90	48	38	31	30	30
**Mixture (0 °C)	41	25	28	24	15	7	19	11
$AsCl_3$ (25 °C)	22	48	34	48	67	82	90	90
Mole fraction of PCl_3 in mixture	1.0	1.0	1.0	1.0	1.0	1.0	0.2	0.1
Composition calculated from flow rates (% P)	87.0	65.4	75.0	64.5	44.7	23.1	13.2	4.2
Growth time (hr)	6	8	8	5.75	6	6	6.25	6.5
Epitaxial layer:								
Thickness (μ) (111)	150-300	400	600	425	425	425	450	450
$(\overline{111})$	75	100						
Growth rates (μ/min) (111)	0.4-0.8	0.8	1.25	1.25	1.2	1.2	1.2	1.15
$(\overline{111})$	0.2	0.2						
Lattice constant (Å)	5.481	5.520	5.500	5.515	5.556	5.582	5.617	5.642
Composition from lattice data (% P)	85.0	65.5	72.0	67.5	48.0	35.0	17.7	5.4
Energy gap [for $\alpha = 10\ cm^{-1}$ at 300 °K] (ev)	2.13	2.02	2.07	2.05	1.88	1.72	1.57	1.42
Free carrier absorption in infrared	none	some	none	none	none	none	none	none

*With a gradient of 16 °C/cm.

**Mixture of $AsCl_3$ and PCl_3.

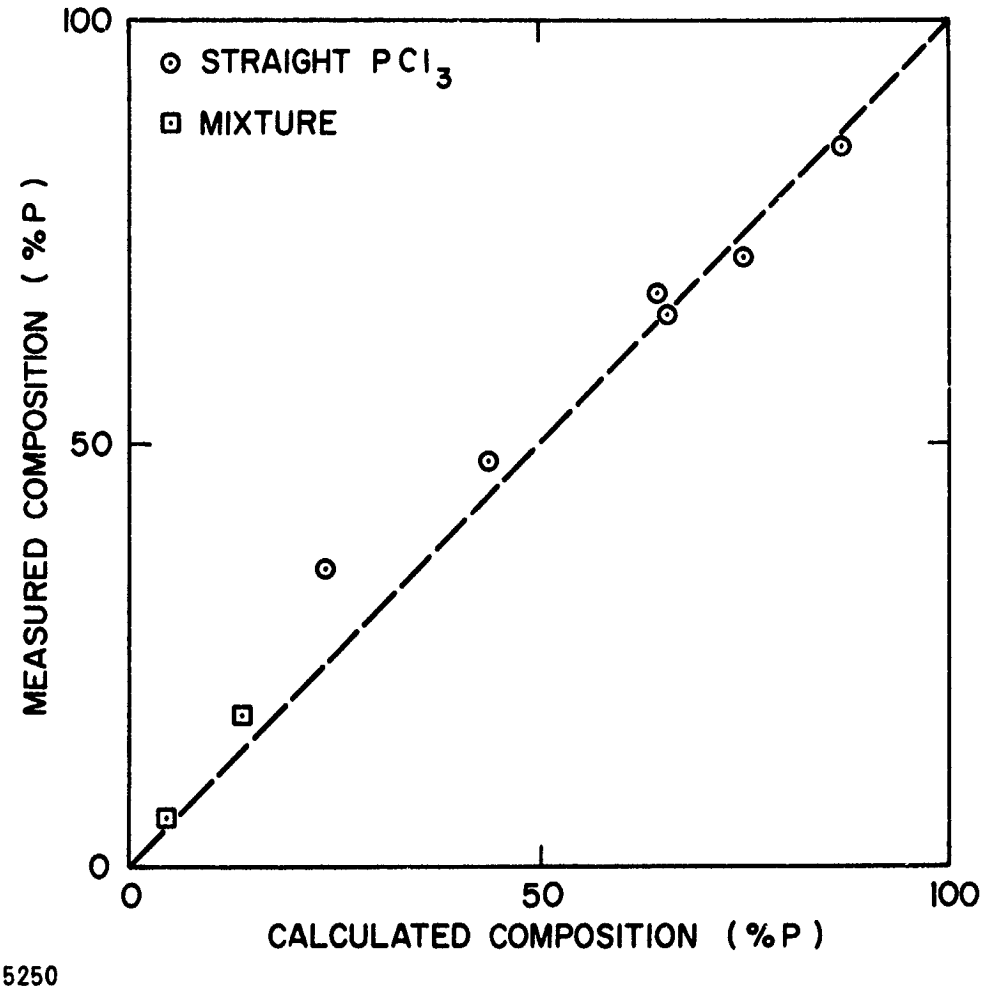

FIG. 5. EVALUATION OF COMPOSITION OF THE ALLOY.

mixture of PCl_3 and $AsCl_3$, instead of pure PCl_3, in one of the bubblers to reduce the vapor pressure of PCl_3 to such a value that adequate flow rate could again be applied. The improvement is clearly indicated in runs 28 and 29, where the calculated composition is obtained by assuming that the partial pressure of PCl_3 is equal to the mole fraction of PCl_3 times the vapor pressure of the pure substance (Henry's law [Ref. 8] with $\gamma = 1$).

b. The optimum flow rates were determined experimentally. It was found that a total transport of 5×10^{-5} to 9×10^{-5} mole/min of halides and that a total flow of 120 to 150 cc/min of H_2 were best for the 1-in. ID reaction tube.

c. The growth rate on the (111)A surface of GaAs was not only smoother but also faster than that on the (111)B surface; the ratio was 4 to 1. The opposite was reported by Gibbons and Prehn [Ref. 4]. These observations can be best appreciated by the pictures presented in Fig. 6. The two epitaxial layers were grown in a single run with the substrate standing parallel to the flow of gas so that both surfaces were under the same growth conditions. The best result was obtained with a growth rate of 1.2 μ/min or 0.5 mm in seven hours on the (111)A surface of GaAs.

d. Alloy crystals with x ranging from 0 to 1 were successfully grown within a very narrow temperature region, from 800 to 825 ^{o}C. The inclined position of the substrate in the growth zone with a temperature gradient of 16 ^{o}C/cm resulted in at least a 10 ^{o}C difference between the leading and the trailing edges of the substrate along the length of the tube. However, the X-ray diffraction and the band-edge absorption (see Section D) showed that there was no composition gradient across the grown crystal. It is clear that the composition is entirely determined by the ratio of hydrogen flow rates through the halides and is not sensitive to the temperature at which the crystal is grown. Thus the growth process is extremely reproducible. Furthermore, it is possible to achieve fast growth with a very steep temperature gradient without affecting the homogeneity of the alloy crystal.

e. The phosphorus-rich epitaxial layers were usually cleaved along the (110) directions [Ref. 9] as a result of lapping on the substrates. Etching was used to remove the GaAs substrate from the epitaxial layer for compositions up to 65 percent arsenic. The etchant was a mixture of 1 part HNO_3 and 1 part HF. For alloys of more than 65 percent arsenic in composition, the substrates were removed by lapping. No cleavage in the epitaxial layer was found since the mismatch in lattice constant at the interface between GaAs and the GaAs-rich layer was not serious.

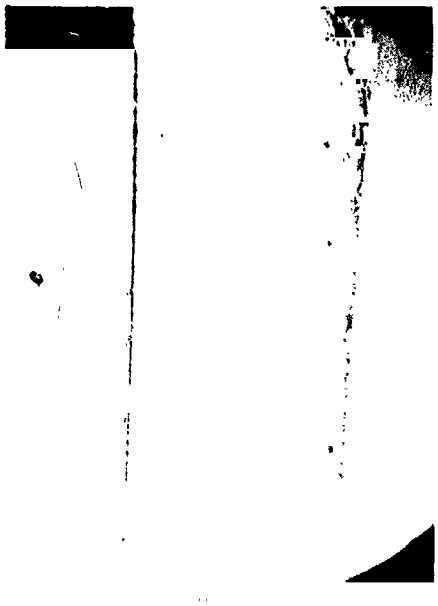

a. Thickness of epitaxial layers (gray regions) on the (111)-oriented GaAs substrate. Crystal grown on the A surface is shown on the right side; that on the B surface, the left side.

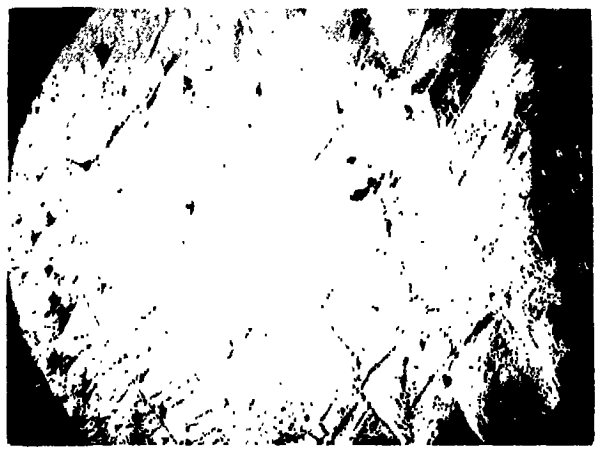

b. Crystal grown on (111)A surface of GaAs

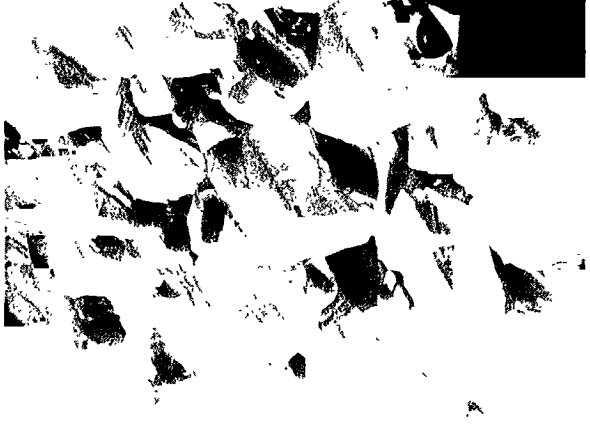

c. Crystal grown on (111)B surface of GaAs

FIG. 6. APPEARANCE OF CRYSTALS AFTER GROWTH.

D. MEASUREMENTS

The following measurements were made to determine the homogeneity in the composition and the free carrier concentration of the epitaxially grown alloy crystals.

1. X-ray Diffraction Measurement

The alloy crystals were known to be single crystals by the surface appearance as well as the perfect cleaved edges in the (110) directions [Ref. 9]. The lattice constant and the homogeneity of the crystals were determined from X-ray diffraction patterns of powdered samples. A GE XRD-1 spectrometer was used in the study. Silicon powder was mixed with the sample powder as the reference material. Cu $K\alpha_1$ radiation gave a Si (440) line at $2\theta_B = 106.72$ deg and a Si (531) line at $2\theta_B = 114.12$ deg [Ref. 10], where θ_B is the Bragg angle. The (531) line of the alloy crystal was located between the two Si lines. The accuracy of measurement in the lattice constant was $\pm 2.5 \times 10^{-4}$ Å, and that of the composition x was ±0.1 percent. A typical X-ray diffraction pattern is shown in Fig. 7, in which all three diffraction lines are plotted. Notice that the Cu $K\alpha_1$ and $K\alpha_2$ lines are resolved at

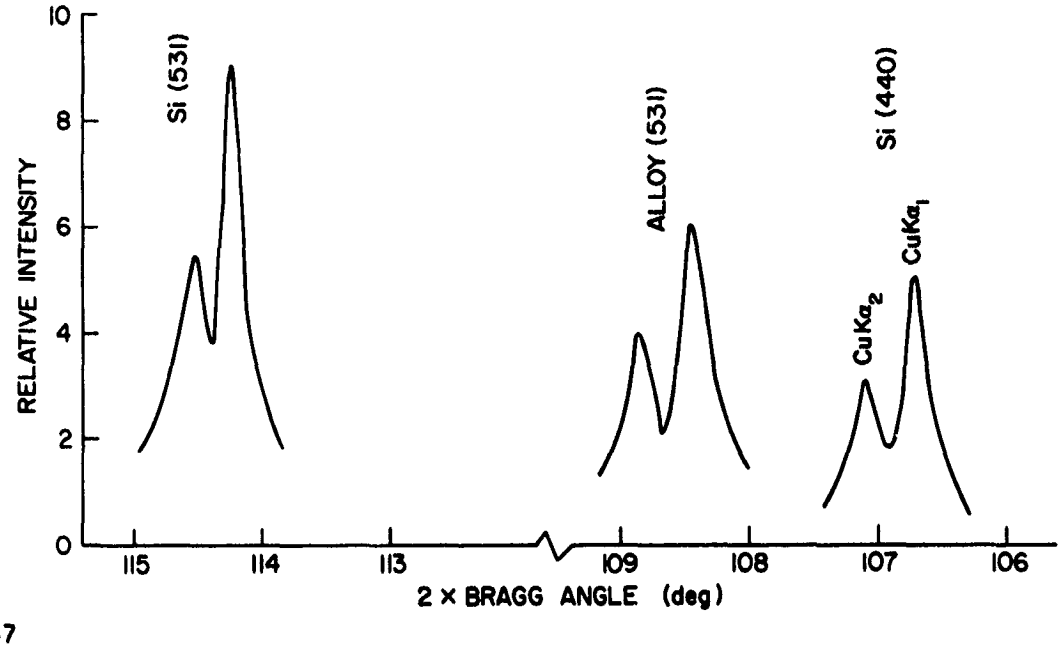

FIG. 7. X-RAY DIFFRACTION PATTERN OF POWDERED SAMPLE ($GaAs_{0.946}P_{0.054}$ + Si).

these high Bragg angles. By comparing the width of the diffraction lines from the alloy and from silicon, it was concluded that the material grown was extemely homogeneous. By studying the samples obtained from different portions of a given alloy crystal, it was found that the composition varied no more than ±0.25 percent.

2. Band-Edge Absorption

For semiconductors with the conduction band minimum at $\vec{k} \neq 0$ in the Brillouin zone, the absorption coefficient of the indirect band-edge transition α obeys the following relation [Ref. 11]:

$$\alpha = \text{const}\left[\frac{(h\nu - \mathcal{E}_g - \mathcal{E}_p)^2}{1 - \exp(-\mathcal{E}_p/kT)} + \frac{(h\nu - \mathcal{E}_g + \mathcal{E}_p)^2}{\exp(\mathcal{E}_p/kT) - 1}\right] \qquad (2.3)$$

for $h\nu > \mathcal{E}_g + \mathcal{E}_p$, where $\mathcal{E}_g$ is the band gap, $\mathcal{E}_p$ is the energy of the phonon involved in the transition, and $h\nu$ is the energy of the incident photon. The first term of Eq. (2.3) is contributed by phonon emission and the second, by phonon absorption. The former drops out for $h\nu < \mathcal{E}_g + \mathcal{E}_p$; finally the latter drops out for $h\nu < \mathcal{E}_g - \mathcal{E}_p$ and α becomes zero from there on. A plot of $\alpha^{\frac{1}{2}}$ vs $h\nu$ gives a straight line for $h\nu > \mathcal{E}_g + \mathcal{E}_p$ [Ref. 11]. Measurements of the band-edge absorption were made at 300 ^{o}K on the phosphorus-rich samples which were known to have indirect energy gaps; and a typical result of $\alpha^{\frac{1}{2}}$ vs $h\nu$ is given in Fig. 8 for a sample of 67.5 percent of phosphorus. A slope of 140 cm^{-1} ev^{-1} is obtained from the straight-line portion of the curve; this result is comparable to the value reported for pure GaP at 300 ^{o}K [Ref. 12]. This is additional evidence of the homogeneity of the crystals grown by this process.

3. Investigation of Carrier Concentration

A simple way of investigating the carrier concentration is by observing the free carrier absorption in the near-infrared region; such absorption cannot be tolerated, for it will override the lattice absorption in the multiphonon absorption region and it will also cause a shift in the structure of the Reststrahlen band [Ref. 13]. It is clear that

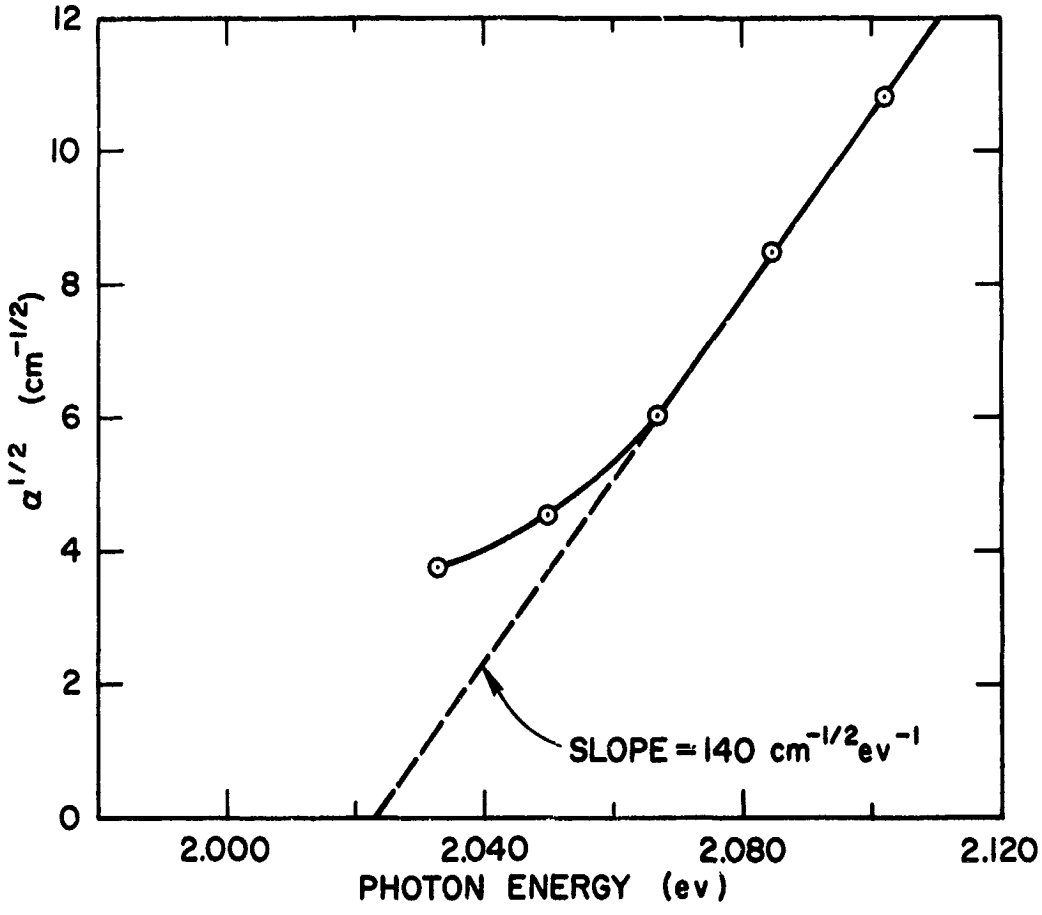

FIG. 8. SQUARE ROOT OF ABSORPTION COEFFICIENT VS PHOTON ENERGY AT BAND EDGE OF $GaAs_{0.325}P_{0.675}$.

the criterion is the absence of free carrier absorption at 300 ^{o}K rather than a certain upper limit of the carrier concentration, although the two are quite related [Ref. 13]. Transmission data of these alloy crystals in the wavelength region of 1μ to 12μ gave absolutely flat characteristics, indicating that there was no appreciable absorption.

Hall measurements were made by others [Ref. 14] on similar materials. The results on undoped GaP crystals showed that the resistivity was of the order of 600 ohm-cm N-type, that the electron mobility was greater than 150 cm^2/volt-sec, and that the electron concentration n_o was therefore less than 10^{14} cm^{-3}. The electron concentration of undoped GaAs crystals was found to be lower than 10^{15} cm^{-3}.

III. INTERACTION OF PHONONS WITH PHOTONS

A number of techniques utilizing the interaction of phonons with external radiation can be used to detect the phonon spectrum of a crystalline solid. These interactions are interesting in their own right in that they depend on the intrinsic properties of the crystal. The simultaneous requirements for conservation of energy and momentum in any photon-phonon interaction place a severe limit on the types of interaction that are possible. Phonon energies are usually less than 0.1 ev and their wavelengths usually less than 10 Å; photons of similar energies lie in the infrared region, whereas those of comparable momentum lie in the X-ray region of the radiation spectrum. For this reason, the most useful technique in determining the phonon spectrum does not depend on photon-phonon interactions but on inelastic scattering of thermal neutrons, since such neutrons have energies and momenta comparable with those of phonons. The entire phonon spectrum can be determined from neutron scattering techniques. However, the interaction of photons with phonons in the infrared region remains a very important means for studying the phonon spectrum, particularly when neutron scattering data are not readily accessible. Such interaction also provides information about the intrinsic properties of the crystal. With the development of high-resolution infrared spectroscopy and high-purity semiconductors, such interactions have been measured in sufficient detail to yield useful information.

The interactions can be separated into two major processes: (1) single-phonon interaction, that is, the excitation of the transverse optical phonons of zero wave vector in polar crystals; and (2) multi-phonon interaction, that is, the excitation of two or more phonons of any wave vector provided momentum is conserved. Both of these processes occur in the infrared region of the spectrum. This chapter is concerned with existing theories related to the above two types of interactions in ordered solids, particularly in semiconductors of zinc blende structure. Similar interactions will be investigated in the alloy system $GaAs_xP_{1-x}$ in subsequent chapters.

A. PHONON SPECTRUM

The term "phonon" has been created as an analog to the name "photon" to emphasize the similarities between both the classical and quantum-mechanical theories of sound and light waves. A phonon is a normal mode of vibration of the crystal and is defined as an eigenstate of momentum represented by a traveling plane wave of wave vector $\vec{k}$ in the crystal. For a crystal containing N unit cells, there are N possible momentum eigenstates distributed evenly throughout the first Brillouin zone in such a way that the number of eigenstates along a certain direction in the zone is equal to the number of unit cells along that particular direction in the crystal. Crystals of zinc blende structure, to which GaAs and GaP belong, contain two atoms in each unit cell. The crystal has a total of 6N degrees of freedom of vibration; this means that for each value of $\vec{k}$ in the zone there are six associated energy eigenstates. In terms of the three-dimensional Brillouin zone, these energy eigenstates form six phonon dispersion surfaces. The cross sections of these surfaces of GaAs [Ref. 15] are shown as branches in Fig. 9 at various crystal momentum directions [including $\Gamma(0,0,0)$, $X(1,0,0)$, $L(\frac{1}{2},\frac{1}{2},\frac{1}{2})$, and $W(1,\frac{1}{2},0)$]. Of these six branches, three approach zero as $\vec{k}$ goes

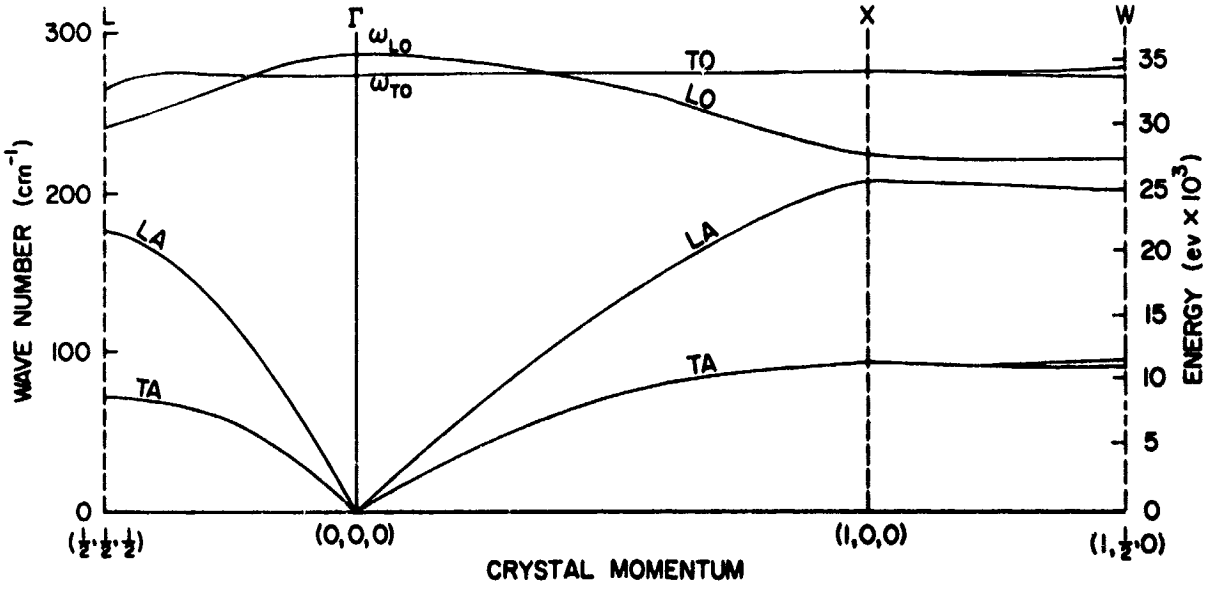

35252

FIG. 9. PHONON SPECTRUM OF GaAs (CALCULATED BY JOHNSON AND COCHRAN, REF. 15).

to (0,0,0), while the other three approach finite energy values. The former are called acoustical branches and consist of two transverse (TA) and one longitudinal (LA) modes; the latter are called optical branches and also consist of two transverse (TO) and one longitudinal (LO) modes. Both the TA and the TO modes are generally degenerate.

Furthermore, in the case of zinc blende crystals, the LO and the TO modes are separated at both Γ and X with the result that the entire LO branch moves to higher energies; the frequency of the LO(Γ) phonon (LO phonon at the Γ point), ω_{LO}, is larger than that of the TO(Γ) phonon, ω_{TO}, as shown in Fig. 9. This is due to the longitudinal polarization field $E_L = -4\pi P_L$ (where P_L is the longitudinal polarization), which is induced by the LO mode and which adds an additional harmonic restoring force to the LO mode. The corresponding transverse polarization field is absent. This longitudinal polarization comes about by the charge transfer between the two atoms in the unit cell resulting in a linear electric moment in the cell. Since this linear moment is absent in crystals having the diamond structure, the lattice vibrations make no contributions to the dielectric constant and therefore $\omega_{LO} = \omega_{TO}$.

B. SINGLE-PHONON INTERACTION

In order for interaction between photons and phonons to occur, the following three requirements must be satisfied:

1. Conservation of momentum between the initial and final states.
2. Conservation of energy between these states.
3. A coupling mechanism between radiation field and vibrational modes.

As mentioned in Section A, there is a charge transfer between the two atoms in the unit cell of a zinc blende crystal. A linear electric moment thus exists which gives rise to a first-order dipole transition resulting in the absorption (or emission) of photons by phonons. As for the conservation of momentum and energy, the following are required: $\omega_o = \omega_j$ and $\vec{k}_o = \vec{k}_j$, where $\omega_o, \vec{k}_o$ and $\omega_j, \vec{k}_j$ are respectively the frequencies and wave vectors of the photons and phonons of the j^{th} branch. The selection rule is $\Delta n(\vec{k}_j) = \pm 1$, where $n(\vec{k}_j)$ is the

occupation number of the j^{th} branch of the phonon spectrum at $\vec{k}_j$. In the dipole transition, the first-order matrix elements involve the factor $\vec{d}_j \cdot \vec{f}$ [Ref. 16], where $\vec{d}_j$ is the polarization vector of the phonon in branch j and $\vec{f}$ is that of the photon. Therefore, the coupling matrix will only yield nonzero values for the TO phonons. In addition, since photons of these frequencies have essentially zero wave vectors, only the TO(Γ) phonons are involved in the photon absorption (or emission) process. Thus $\omega_j = \omega_{TO}$ and $\vec{k}_j = \vec{k}_{TO} \tilde{=} 0$, where $\vec{k}_{TO}$ is the wave vector of the TO(Γ) phonon. This process is shown in Fig. 10.

To sum up, the absorption of photons by TO(Γ) phonons (called fundamental absorption) is a strong first-order process; thus the absorption coefficient is large and of the order of 10^4 cm^{-1} or more for GaAs [Ref. 17]. Furthermore, since the wavelength of radiation is very large compared with the size of a unit cell, a classical approach is possible and the problem can be considered as a resonant interaction between radiation and damped electric oscillator [Ref. 18] as shown in the appendix.

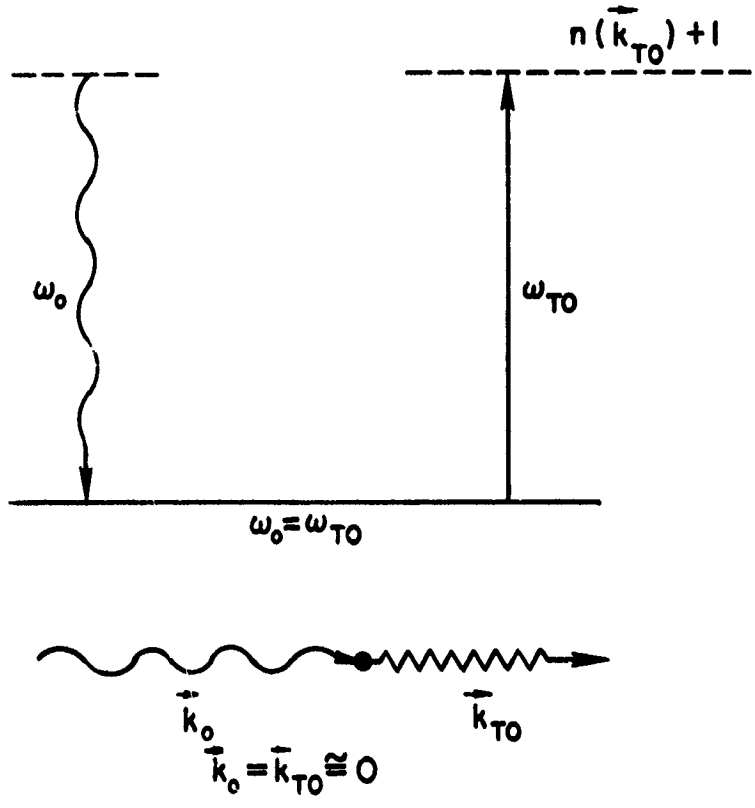

FIG. 10. CONSERVATION OF ENERGY AND MOMENTUM OF THE FIRST-ORDER PHOTON-PHONON INTERACTION.

C. MULTIPHONON INTERACTION

Interactions between a photon and two or more phonons can take place as second or higher order processes. In the two-phonon process, the energy and momentum conservations are satisfied by having $\omega_o = \omega_j \pm \omega_{j'}$ and $\vec{k}_o = \vec{k}_j \pm \vec{k}_{j'}$, where j and j' are the two branches of the phonon spectrum. In the case of the photon absorption the plus sign signifies the creation of a phonon and the minus sign indicates the annihilation of a phonon.

Two coupling mechanisms of interaction have been proposed. The first--arising from the second-order electric moment in the crystal--was introduced as the major mechanism in diamond-type semiconductors [Lax and Burstein, Ref. 19]. In this scheme of interaction one phonon induces a change in effective charge on neighboring atoms, which are then displaced by a second phonon to produce an electric moment which in turn interacts with the radiation (see Fig. 11).

The second one [Kleinman, Ref. 20] was introduced as the major mechanism in zinc blende gallium phosphide. The essential point of the theory is that a $TO(\Gamma)$ phonon is created by the radiation field as an intermediate state, and then the $TO(\Gamma)$ phonon scatters into two phonons under the perturbing influence of the cubic anharmonic terms in the crystal potential. The momentum conservation is satisfied throughout the process, that is, between initial and intermediate states and between intermediate and final states; on the other hand, energy conservation is required only between the initial and final states. This scheme of interaction is depicted in Fig. 12.

The latter mechanism is not applicable to diamond-type crystals due to the absence of a first-order electric moment; however, both mechanisms can be applied to zinc blende crystals, although the latter are believed to be dominant on account of the much larger absorption. Clearly, from either mechanism the absorption of photons is strong whenever the combined density of states of phonons is high, provided the selection rule does not forbid such interactions. Thus it is expected that most structures in the absorption spectra will be related to phonons near the Brillouin zone boundaries, where $d\omega/dk_i = 0$ (with i being an arbitrary

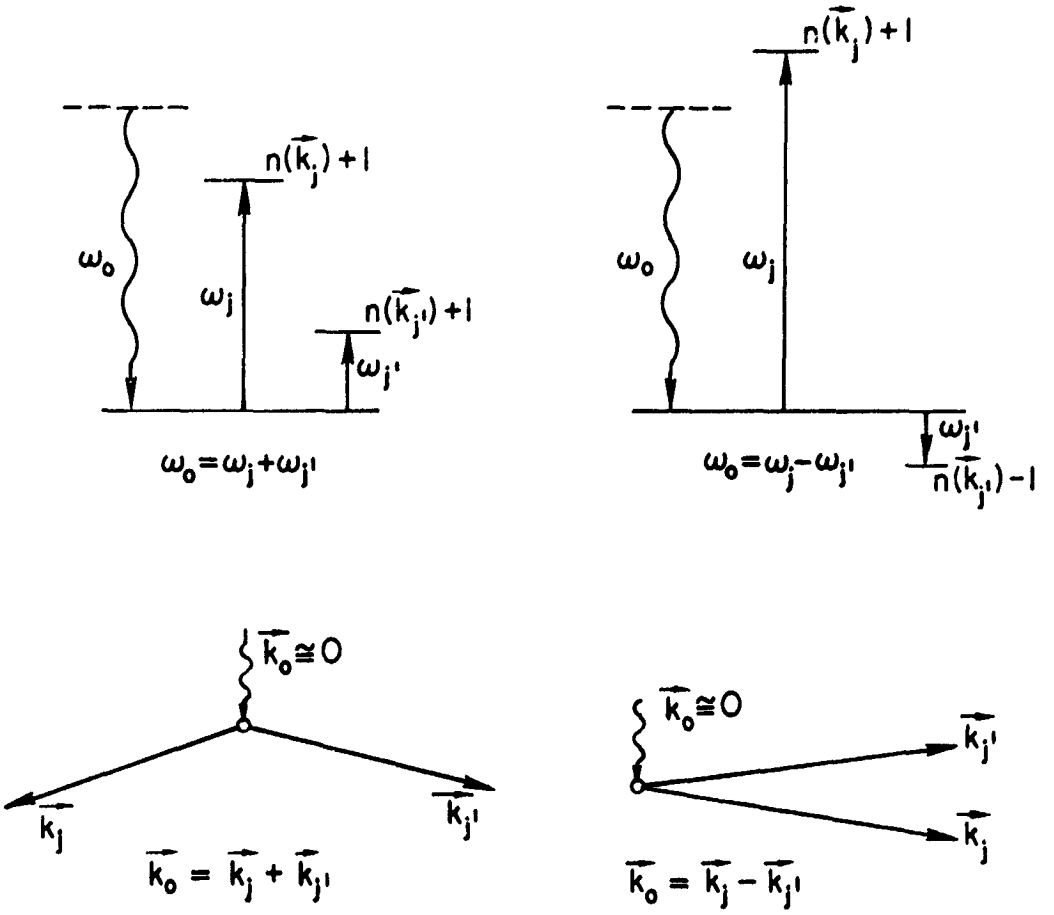

a. Summation process

b. Difference process

FIG. 11. CONSERVATION OF ENERGY AND MOMENTUM OF THE SECOND-ORDER PHOTON-PHONON INTERACTIONS DUE TO SECOND-ORDER ELECTRIC MOMENT.

direction) for most branches (surfaces) in the zone. As for the selection rules, they depend strongly on the symmetry of the crystal and it is possible to deduce them at the critical points from space group symmetry [Ref. 21].

Since the matrix elements of either mechanism do not change significantly with temperature, the temperature dependence of the absorption process is then entirely contributed by the changes in the occupation number $n(\vec{k}_j)$, which is given at thermal equilibrium by the well-known Bose-Einstein equation:

$$n(\vec{k}_j) = \left\{ \exp\left[\frac{\hbar\omega(\vec{k}_j)}{kT}\right] - 1 \right\}^{-1} \qquad (3.1)$$

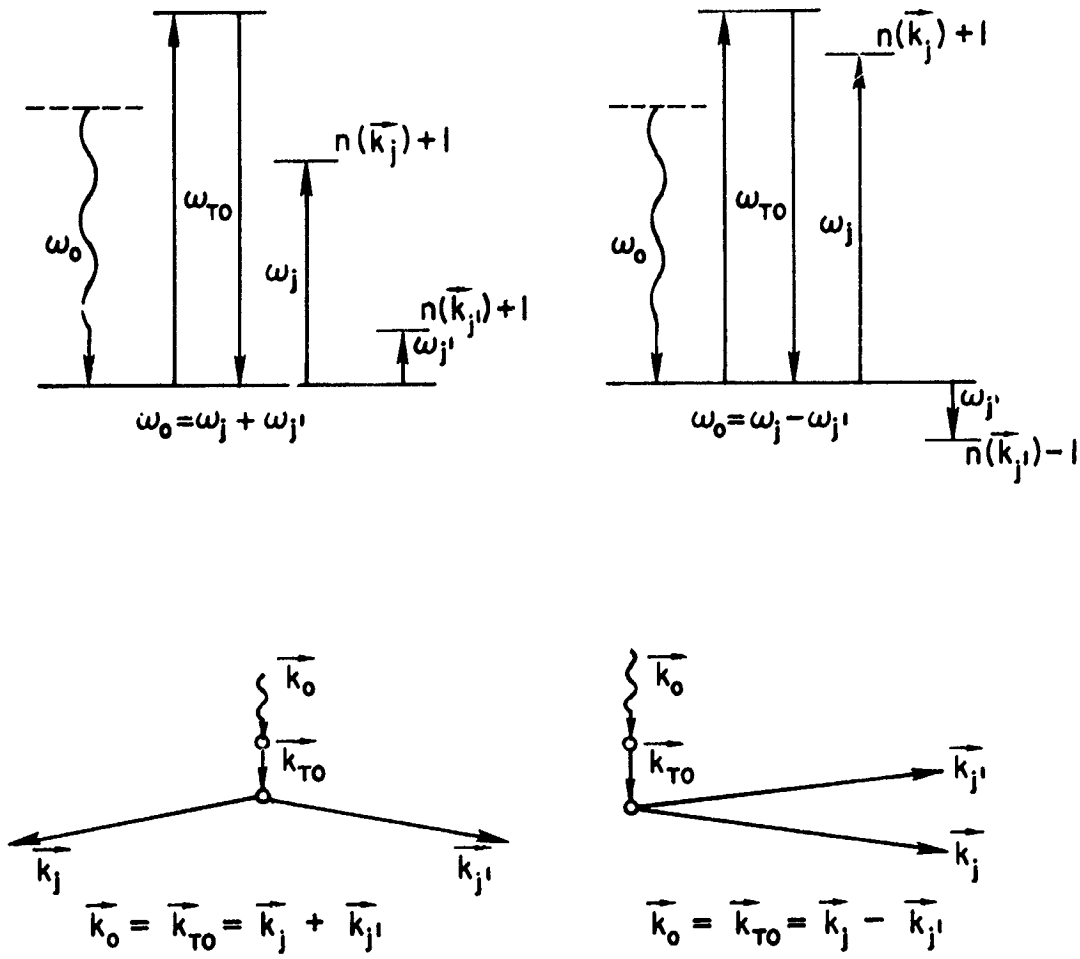

35256

a. Summation process b. Difference process

FIG. 12. CONSERVATION OF ENERGY AND MOMENTUM OF THE SECOND-ORDER PHOTON-PHONON INTERACTIONS DUE TO ANHARMONIC COUPLING.

In the case where two phonons are created simultaneously by the radiation (summation process), the temperature dependence of the absorption is

$$f(T) = [1 + n(\vec{k}_j)][1 + n(\vec{k}_{j'})] - n(\vec{k}_j)\, n(\vec{k}_{j'}) , \qquad (3.2)$$

which is essentially proportional to the difference between the stimulated absorption and the stimulated emission. In the case where one phonon is created and the other is destroyed (difference process), the dependence is

$$f(T) = [1 + n(\vec{k}_j)]\, n(\vec{k}_{j'}) - n(\vec{k}_j)[1 + n(\vec{k}_{j'})] . \qquad (3.3)$$

It is important to recognize that these interactions are of second order and that the absorption strength is weak compared to that described in Section B. Since the phonons involved are near zone boundaries, the vibrational wavelengths are of the order of one lattice constant, so that they are extremely small compared to those of phonons near the zone center. By studying the multiphonon absorption spectra of a disordered system such as those in $GaAs_xP_{1-x}$ alloy crystals, it may thus be possible to deduce some basic knowledge relating to the nature of disorder (or order) in the microscopic sense.

IV. EXPERIMENTAL STUDY OF RESTSTRAHLEN BANDS IN $GaAs_xP_{1-x}$

A. INTRODUCTION

The experimental work described in this chapter is concerned with first-order photon-phonon interactions in $GaAs_xP_{1-x}$. Because of the high absorption coefficient for this process, detection through transmission measurement would require extremely thin samples of the order of 1 micron, which are very difficult to prepare. The alternative would be to measure the reflectivity spectra in the infrared region. In terms of the optical constants n (the refractive index) and k (the extinction coefficient), the reflectivity R has the value [Ref. 22]

$$R = \frac{(n-1)^2 + k^2}{(n+1)^2 + k^2} \tag{4.1}$$

for normal incidence. The corresponding value of the absorption coefficient α for this process is given from electromagnetic theory [Ref. 22] as

$$\alpha = \frac{4\pi k}{\lambda} , \tag{4.2}$$

where λ is the wavelength. It is thus seen that as α approaches a very large number, approximately 10^4 cm^{-1} [Ref. 17], the value of k will be so large that R approaches unity. This region of nearly total reflection is generally referred to as the Reststrahlen band. The detailed shape of this band in ionic crystals can be treated classically as shown in the appendix, where the frequency of the TO phonon involved in such a transition is shown to be located at resonant frequency ω_0.

Reflectivity measurements were carried out on all the samples of $GaAs_xP_{1-x}$ grown by the method given in Chapter II. The experimental results showed that the TO(Γ) phonons of GaAs and GaP exist simultaneously in the alloy with very little shift in frequency. To the author's knowledge, this new phenomenon has not been previously reported by workers in this field.

B. EXPERIMENTAL PROCEDURE

1. Sample Preparation

Samples with different compositions were grown by the epitaxial vapor growth method. The GaP substrates of these samples were removed from the epitaxial layer by the technique described in Section II.C.3. They were then lapped on both sides with abrasives of successively smaller grit size, the final lapping being done with #3200 grit. A mechanical polishing followed until mirror finish surfaces were obtained; the finished samples had dimensions of approximately 1 cm^2 in area and 15 mils in thickness.

2. Apparatus

Preliminary data were obtained with an optical system consisting of a globar light source, a Leiss single monochromator with a CsBr prism and mirror optics, a Reeder RP-3W thermopile detector with a diamond window, and a phase-sensitive electronic amplifier. The essential features of the spectra were obtained on this system. However, the sensitivity of the system was very poor in the spectral region above 30μ due to the weak source intensity and a significant amount of stray light. The final data were obtained through the cooperation of Professor W. G. Spitzer of the University of Southern California on his infrared spectrometer. This equipment was built around a Perkin-Elmer model 210 filter-grating monochromator covering the range from 7μ to 45μ with four interchangeable gratings whose first-order blaze wavelengths were 7.5μ, 22.5μ, 30μ, and 45μ. Multilayer long-wavelength pass filters were used to confine the operation of the gratings to the first order. The incidence angle on the sample, which was located at the exit-slit side of the monochromator, was 9.5 deg. Precautions were taken to minimize the effects of scattered light and water vapor absorption.

3. Reflectivity Measurements

Data were taken point by point in the spectral region from 20μ to 45μ using gratings of 30μ and 45μ blaze wavelengths. A method of sample-in and sample-out was used to minimize the error due to changes in the environment. Samples of 67.5 and 17.7 percent phosphorus showed interference at the shorter wavelength region which was believed to be

due to reflection from the back surfaces (also polished) and to the absence of free carrier absorption at these wavelengths. However, such intereference disappeared near and throughout the Reststrahlen bands of these samples and data were thus obtained in the region of interest without interference effects. All data were taken at 300 ^{o}K.

C. EXPERIMENTAL RESULTS

Reflectivity spectra were taken on $GaAs_xP_{1-x}$ samples of various compositions. The accuracy of the wave number readings was less than 0.5 cm^{-1}, while the resolution was better than 1 cm^{-1}. In Figs. 13a to 13h the reflectivity values are plotted against the wave numbers in cm^{-1} (defined as $10^4/\lambda$, where λ is the wavelength in microns). Figure 13a is for pure GaAs, Monsanto boat grown, N-type with $n_o = 5 \times 10^{15}$ cm^{-3}; Figs. 13b to 13f are for samples of 5.4, 17.7, 35, 48, and 67.5 percent phosphorus respectively, all grown by the technique described in Chapter II; Fig. 13g is for a sample of 82 percent phosphorus, Merck* grown, N-type with $n_o = 1.69 \times 10^{15}$ cm^{-3}; and finally Fig. 13h is for pure GaP, obtained from the data of Kleinman and Spitzer [Ref. 23] for reference purposes.

The samples of 48 and 67.5 percent phosphorus consisted of several pieces of small crystals, and the discontinuity in the reflectivity spectra near 280 cm^{-1} was due to a change in gratings at this wave number. It is seen, from the reflectivity spectrum of pure GaAs presented in Fig. 13a, that the shape of spectra at the maximum is comparable to the data reported by Iwasa et al [Ref. 17] and that the method of surface preparation described in Section B of this chapter is therefore satisfactory.

The major feature of these data is that two reflectivity maxima were observed in the $GaAs_xP_{1-x}$ alloys; one of these is close to the Reststrahlen band of pure GaP, while the other is close to that of pure GaAs. One obvious conclusion is that the TO(Γ) phonons of GaAs and GaP do not merge but exist independently in this alloy system.

---

*Merck and Company, Rahway, N.J.

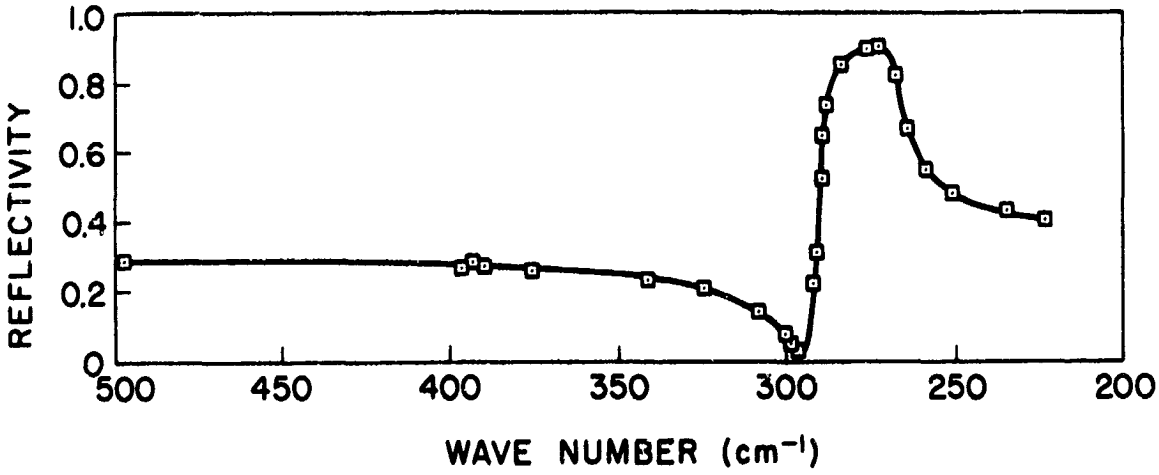

a. GaAs

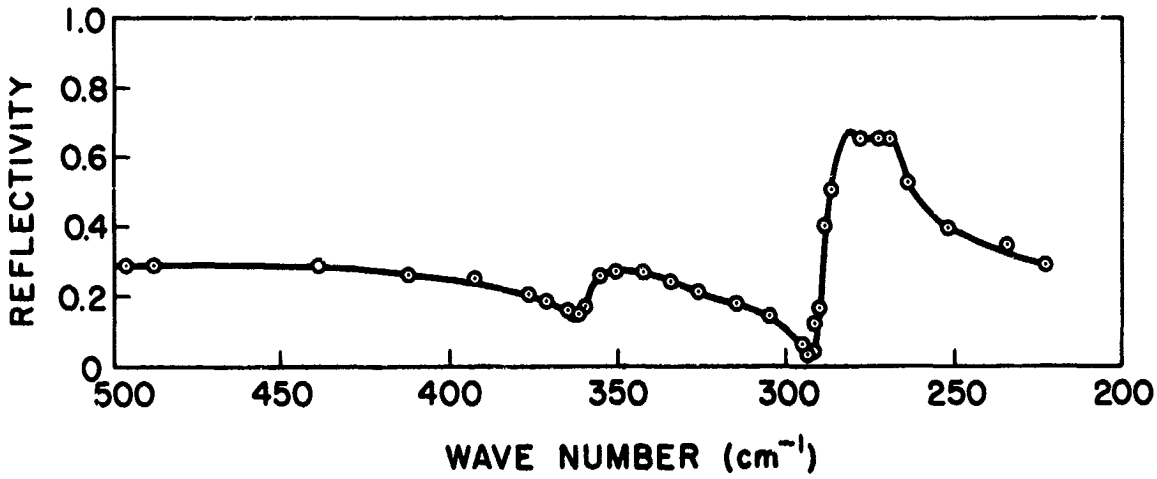

b. $GaAs_{0.946}P_{0.054}$

FIG. 13. REFLECTIVITY VS WAVE NUMBER FOR $GaAs_xP_{1-x}$ AT 300 °K.

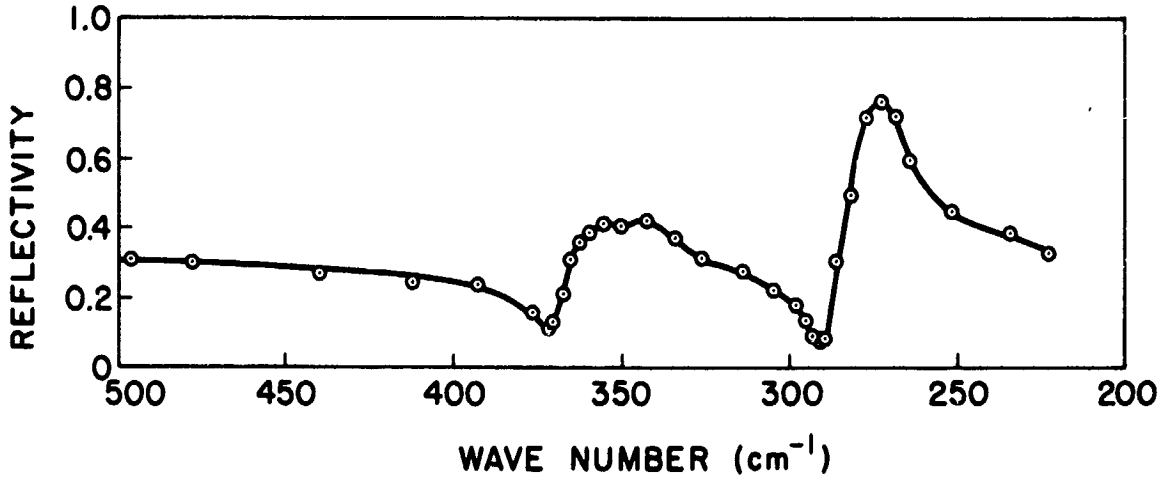

c. $GaAs_{0.323}P_{0.177}$

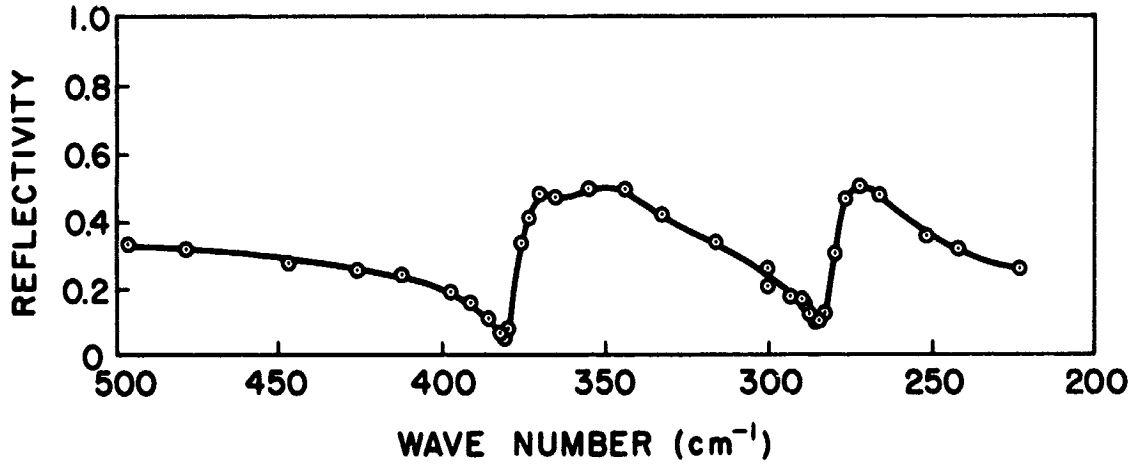

d. $GaAs_{0.65}P_{0.35}$

FIG. 13 (CONTINUED).

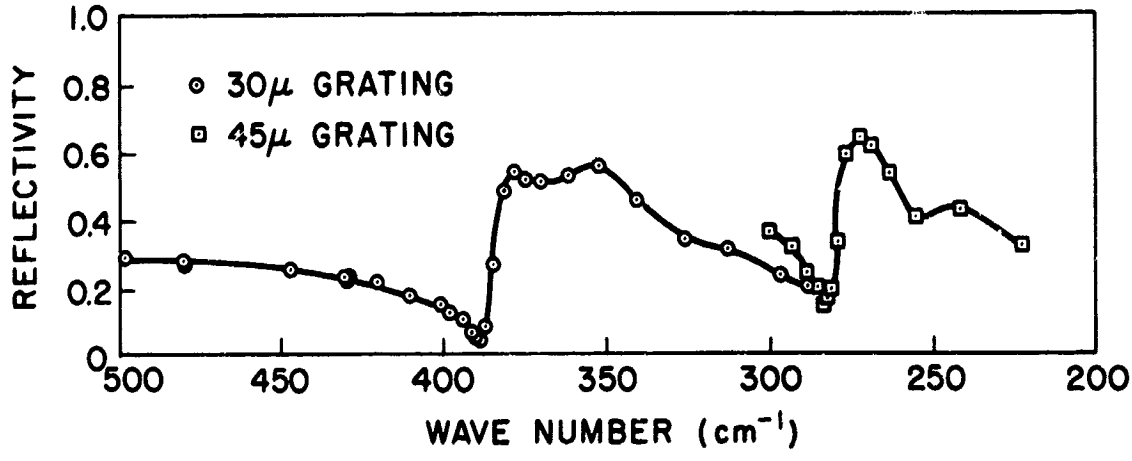

e. $GaAs_{0.52}P_{0.48}$

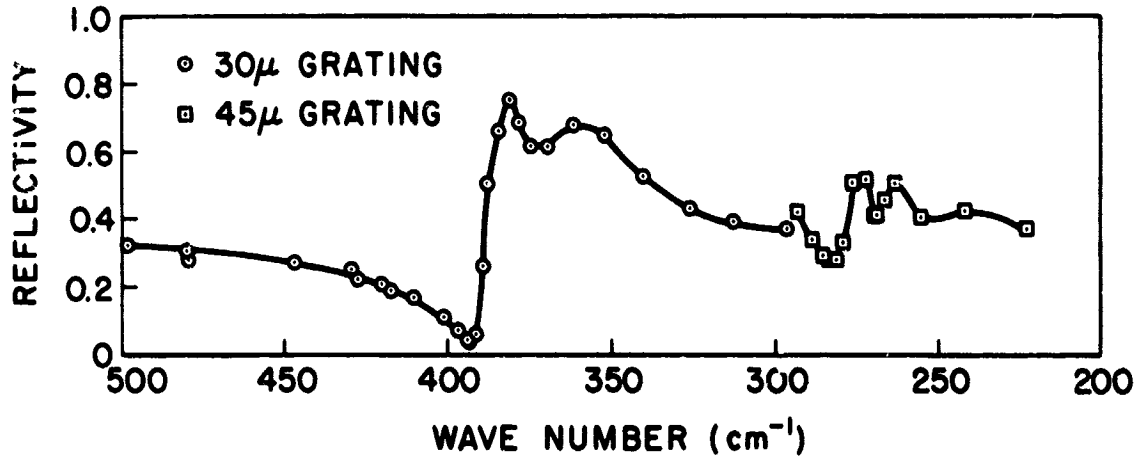

f. $GaAs_{0.325}P_{0.675}$

FIG. 13 (CONTINUED).

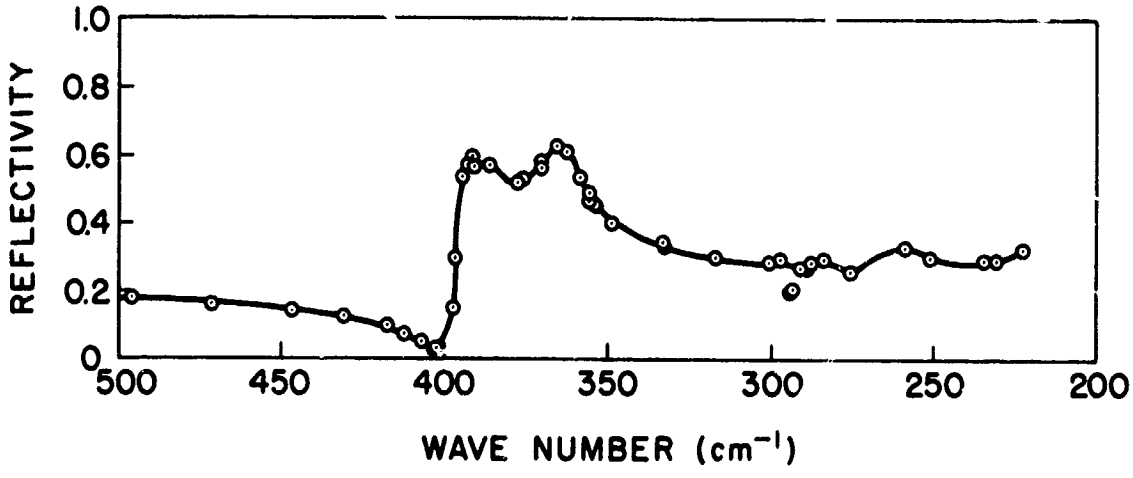

g. $GaAs_{0.18}P_{0.82}$

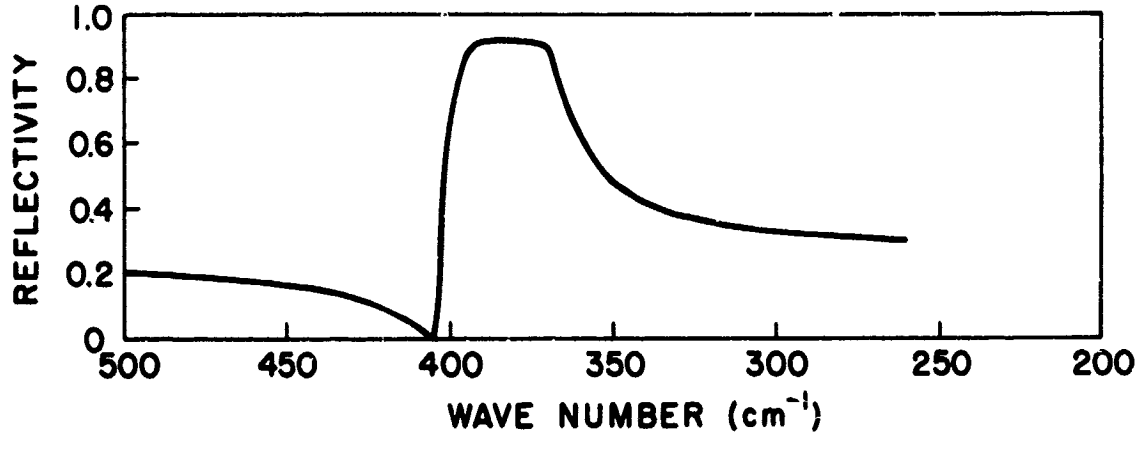

h. GaP [Ref. 23]

FIG. 13 (CONTINUED).

The values of these two resonance frequencies are plotted in Fig. 14 as a function of composition and are also given in Table 2. The frequencies are chosen at the points where the reflectivity maxima begin to decrease on the smaller wave-number side (see appendix), when the shapes of the maxima are square-topped (as is the case for nearly all the GaP-like bands and the GaAs-like bands with x larger than 0.9). The shapes of the maxima for the GaAs-like bands with x less than 0.9 are generally peaked. The frequencies under this condition are chosen at the maximum values. The minima of the reflectivity spectra in the region of the GaAs-like bands tend to shift toward longer wavelength as the mole fraction of arsenic decreases; however, there is very little shift in the Reststrahlen frequency.

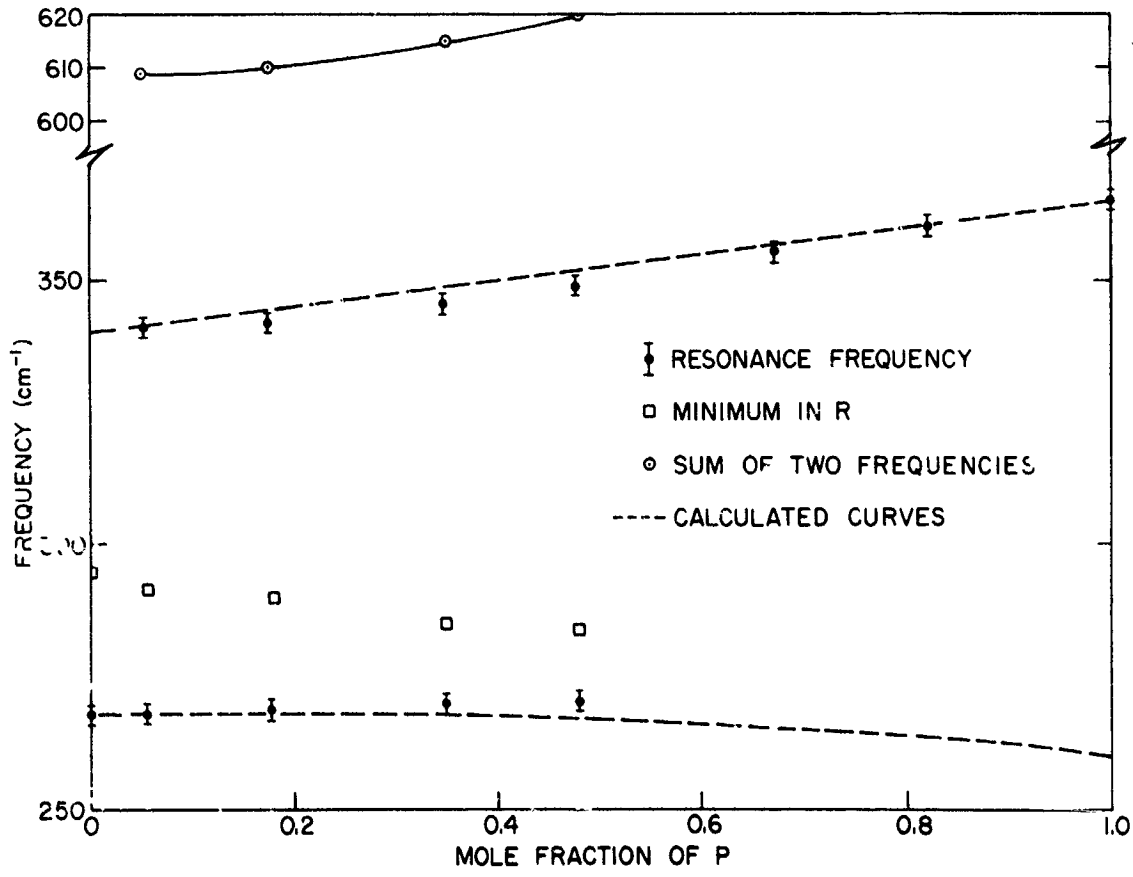

FIG. 14. RESTSTRAHLEN FREQUENCIES OF $GaAs_xP_{1-x}$ AS A FUNCTION OF COMPOSITION.

TABLE 2. MEASURED RESTSTRAHLEN FREQUENCIES OF $GaAs_xP_{1-x}$

Composition (% P)	ω_{TO} of GaP (cm^{-1})	ω_{TO} of GaAs (cm^{-1})
0	--	268
5.4	341	268
17.7	342	269
35	345	270
48	349	271
67.5	355	--
82	360	--
100	366*	--

*From Ref. 23.

D. DISCUSSION

The experimental finding that the TO(Γ) phonons of the constituent materials do not merge into each other but exist simultaneously in the alloy is observed for the first time in this field. Several alloy systems have been studied by others, but opposite results have been reported. For example, Oswald [Ref. 2] studied the Reststrahlen band of $InAs_xP_{1-x}$ and observed that the band shifted continuously from that of InP to that of InAs and was very insensitive to changes of composition in the range from 100 to 20 percent phosphorus. It is felt that the only reason he did not discover a second maximum in the reflectivity spectra is that he had terminated the investigation at 35μ, although the band of InAs is known to be located at about 45μ [Ref. 9]. Transmission data by Potter [Ref. 24] on $GaAs_xSb_{1-x}$ thin films formed by evaporation showed only one absorption peak; however, the crystalline nature of the film was by no means comparable to the single-crystal bulk material used in this work.

1. Theoretical Model

The presence of two reflectivity maxima in the alloy clearly indicates that the classical treatment of interaction of radiation with a single harmonic oscillator is no longer valid. A theoretical treatment is given in Chapter VI to explain how the two eigenfrequencies come about. The experimental results can be fitted excellently with three constants, namely, the force constants of Ga-As, Ga-P bonds as the first nearest neighbors, and that of As-P bond as the second nearest neighbors. This fit is shown by the dashed curves in Fig. 14.

2. Localized Modes

The GaP-like band appears throughout the entire alloy system. As the mole fraction of phosphorus decreases, this band shifts toward smaller wave number and decreases in strength. The GaAs-like band appears only in alloys containing less than 48 percent phosphorus, and its strength also decreases as the mole fraction of As decreases. If the band of the minority constituent is indeed due to the excitation of its vibrational mode in the host lattice of the majority constituent, then the present experimental results agree with the theoretical prediction of Dawber and Elliott [Ref. 25] that only a lighter mass defect (phosphorus in this case) in a heavier host lattice (GaAs-rich lattice in this case) gives certain localized modes appearing with frequencies above the range of unperturbed modes. This phenomenon is clearly indicated by comparing the spectra of 17.7 and 82 percent phosphorus, since they are symmetrically located in composition with respect to $x = 0.50$. It is thus concluded that the nature of the resonance vibration in an alloy such as $GaAs_xP_{1-x}$ is (1) in the form of a TO phonon of zero wave vector for the majority constituent (i.e., a point of the dispersion spectrum in the Brillouin zone), and (2) in the form of a localized mode when that constituent becomes the minority one (presumably a band in the Brillouin zone of the other constituent).

3. "Summation" Band

The sum of the two Reststrahlen frequencies is also given in Fig. 14. It appears near 610 cm^{-1} for x greater than 0.50. It is felt that radiation may interact with the crystal in such a manner that

a photon at this frequency is absorbed and the two Reststrahlen modes are excited simultaneously. Momentum conservation of such an interaction is automatically satisfied since it is satisfied in each separate mode. There is no obvious reason why the matrix element for such a transition should be zero. The strength of this matrix element should be in the order of that of a two-phonon absorption process and should decrease as the mole fraction of phosphorus decreases. This conclusion is based on the assumption that the density of states of the localized modes is proportional to the number of the minority atoms present. It is thus expected that such transitions may be present as an absorption peak in the two-phonon absorption spectra near 610 cm^{-1}. This is indeed so, as will become apparent in Chapter V.

V. EXPERIMENTAL STUDY OF ABSORPTION SPECTRA OF TWO-PHONON SUMMATION BANDS IN $GaAs_xP_{1-x}$

A. INTRODUCTION

The experimental work described in this chapter is concerned with second-order photon-phonon interactions in $GaAs_xP_{1-x}$. Only those absorption bands resulting from the creation of two phonons by the radiation, generally referred to as two-phonon summation bands, were investigated. Such data from GaP and GaAs have been observed by others [Refs. 23, 26]. The reported absorption coefficient of this process is of the order of 10 to 100 cm^{-1}, which makes it possible to study the interactions by the transmission of infrared light through samples of appropriate thickness. The transmittance $\mathcal{T}$ for normal incidence obeys the relation [Ref. 23]:

$$\mathcal{T} = \frac{(1-R)^2 \, e^{-\alpha \ell}}{1 - R^2 \, e^{-2\alpha \ell}} , \qquad (5.1)$$

where ℓ is the thickness of the sample. These bands occur in a region immediately above the Reststrahlen band in wave number; thus to evaluate α from $\mathcal{T}$, reflectivity values at the various wave numbers are needed.

Transmittance measurements were carried out on $GaAs_xP_{1-x}$ samples of various compositions. The absorption coefficients were calculated by means of Eq. (5.1) from the transmittance data and from the reflectivity data reported in Chapter IV. In the absorption spectra of the alloys, a superposition of the two-phonon bands of the pure materials, GaP and GaAs, was observed. This effect indicates that the equivalent modes of the two materials do not merge into each other in the alloy series. The "summation" band suggested in Section IV.D was also observed and it indeed occurred in the vicinity of 610 cm^{-1}.

B. EXPERIMENTAL PROCEDURE

1. Sample Preparation

Samples prepared according to Section IV.B were used. The dimensions of the samples were adequate for the transmittance measurements.

Above all, since there was practically no free carrier absorption in the spectral region of interest, the absorption spectra of the two-phonon summation bands were revealed without interference.

2. Apparatus and Measurement

The apparatus used for these measurements was a Beckman IR-9 spectrophotometer containing a prism-grating monochromator capable of operating in between 2.5μ and 25μ. This equipment could be used either in the single-beam or the double-beam mode. The latter mode was used in our experiments and the resolution was better than 0.5 cm^{-1}. The system was purged with dry nitrogen during operation to reduce the effect of background absorption. The transmittance was measured in the region of 400 to 800 cm^{-1} (25μ to 12.5μ). Although some of the GaAs two-phonon bands fall below this region in wave number, it was possible to obtain the essential features of the spectra of the alloy crystals in this region. All data were taken at 300 ^{o}K.

C. EXPERIMENTAL RESULTS

Absorption spectra of $GaAs_xP_{1-x}$ of various compositions are given in Fig. 15. Figures 15a to 15g are for samples of 100, 85, 67.5, 48, 35, 17.7, and 5.4 percent phosphorus respectively. These samples were all grown epitaxially by the method described in Chapter II. Figure 15h is for pure GaAs, Monsanto boat grown, N-type with $n_o = 5 \times 10^{15}$ cm^{-3}. Spectra of both GaAs and GaP are plotted in Figs. 15b to 15g for comparison.

The GaAs and GaP data compare favorably with the results of Cochran et al on GaAs [Ref. 26] and with those of Kleinman and Spitzer on GaP [Ref. 23]. These authors have given the phonon assignment schemes to the spectra with five phonon energies in each case, the two-phonon bands were identified by their temperature dependence as described in Section III.C. Johnson [Ref. 21] gave alternate assignment schemes to these spectra from a critical point analysis based on the space group symmetry. The assignment schemes are shown in Figs. 15a and 15h, with those by Johnson presented in the brackets. As can be seen, the

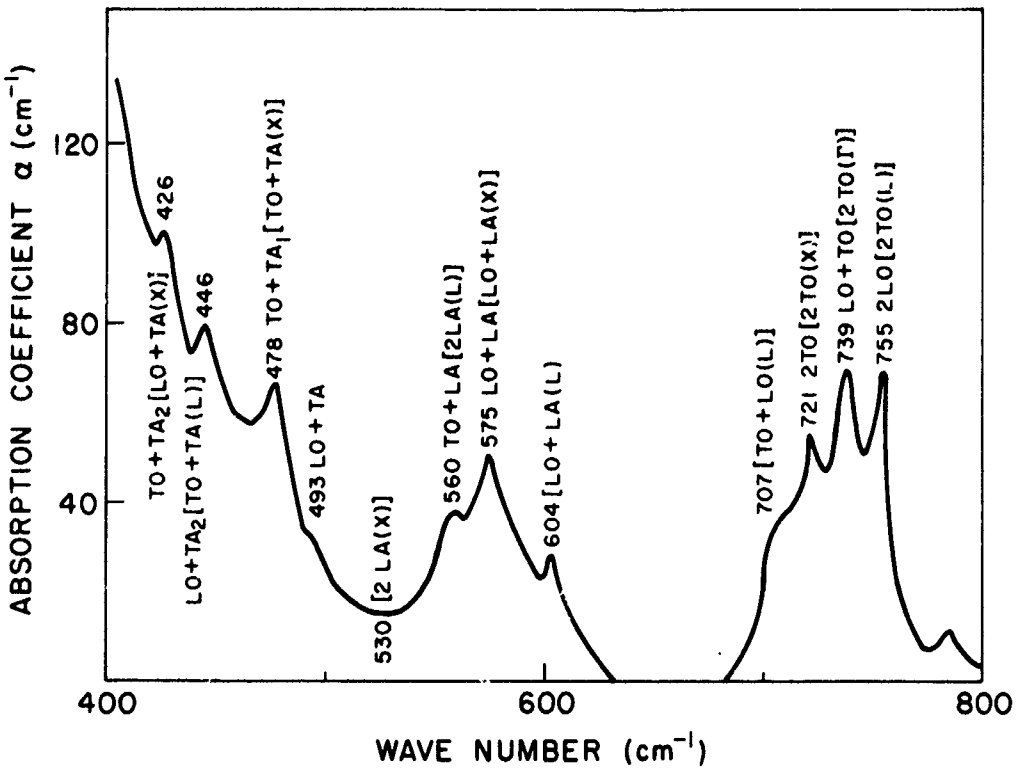

a. GaP. Phonon assignment schemes by Kleinman and Spitzer [Ref. 23] and by Johnson [Ref. 21] are given, with the latter show. inside the brackets.

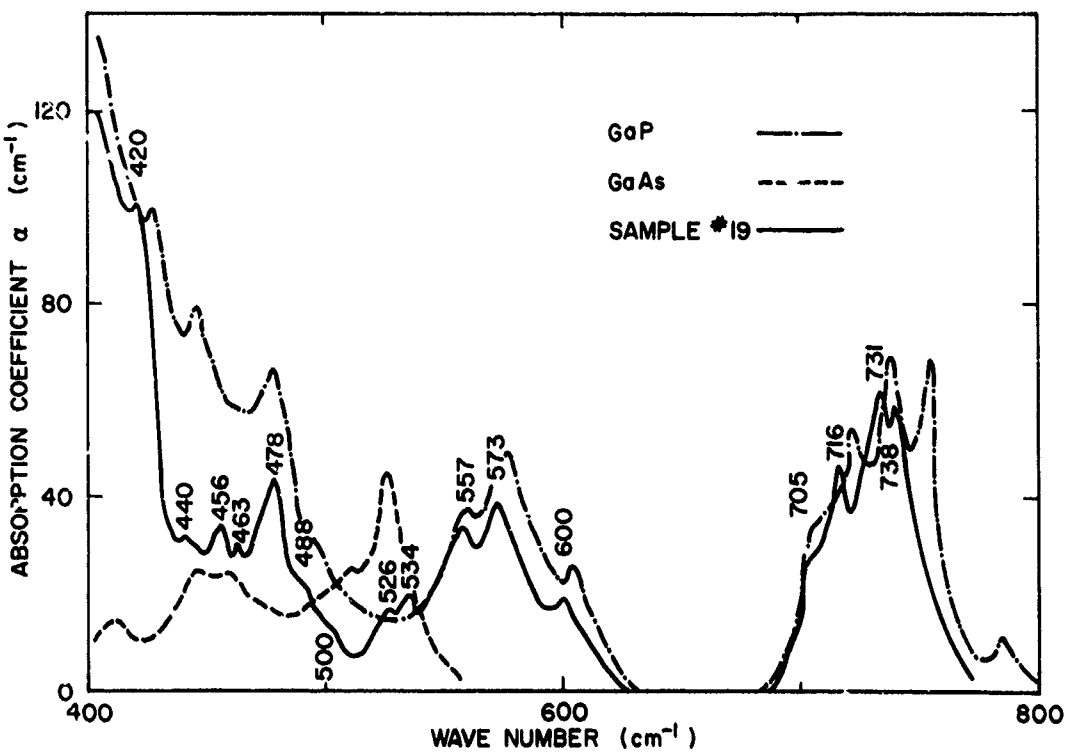

b. $GaAs_{0.15}P_{0.85}$

FIG. 15. LATTICE ABSORPTION SPECTRA OF $GaAs_xP_{1-x}$ AT 300 °K.

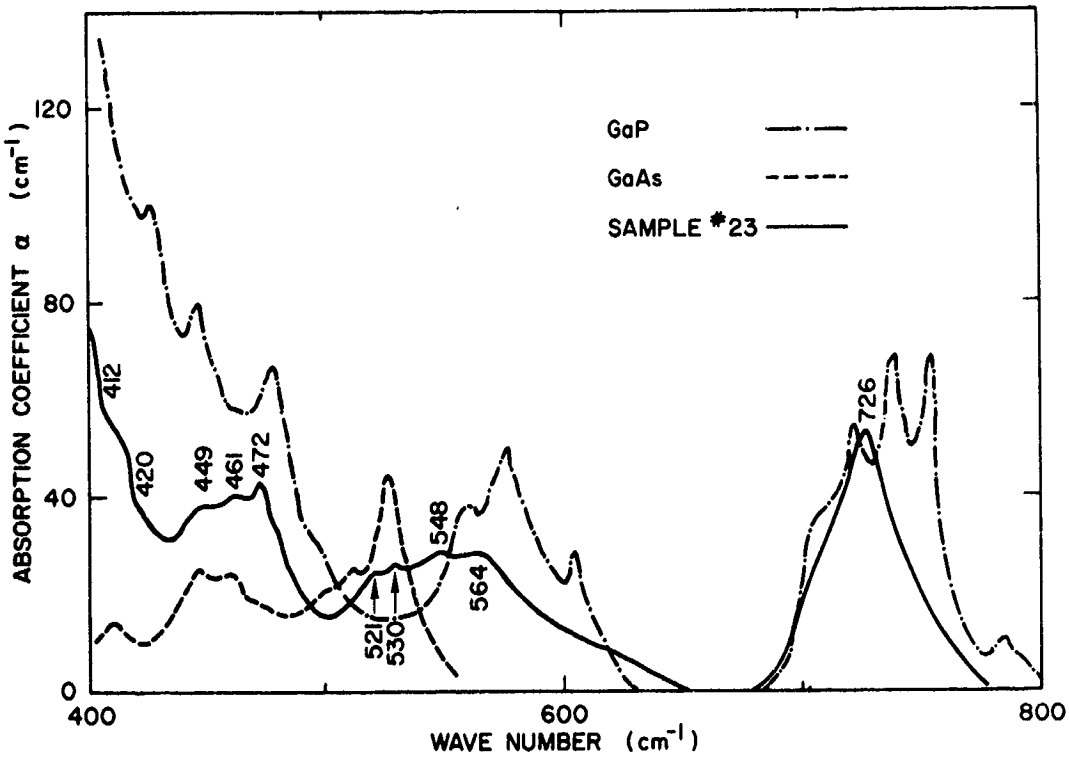

c. $GaAs_{0.325}P_{0.675}$

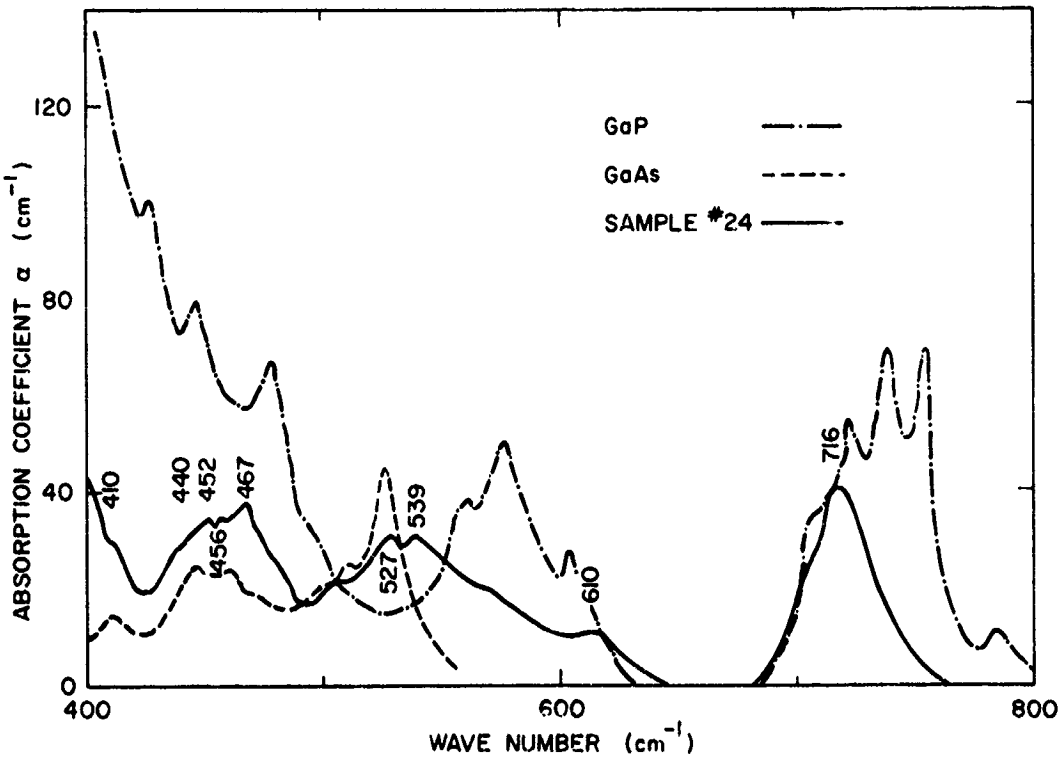

d. $GaAs_{0.52}P_{0.48}$

FIG. 15 (CONTINUED).

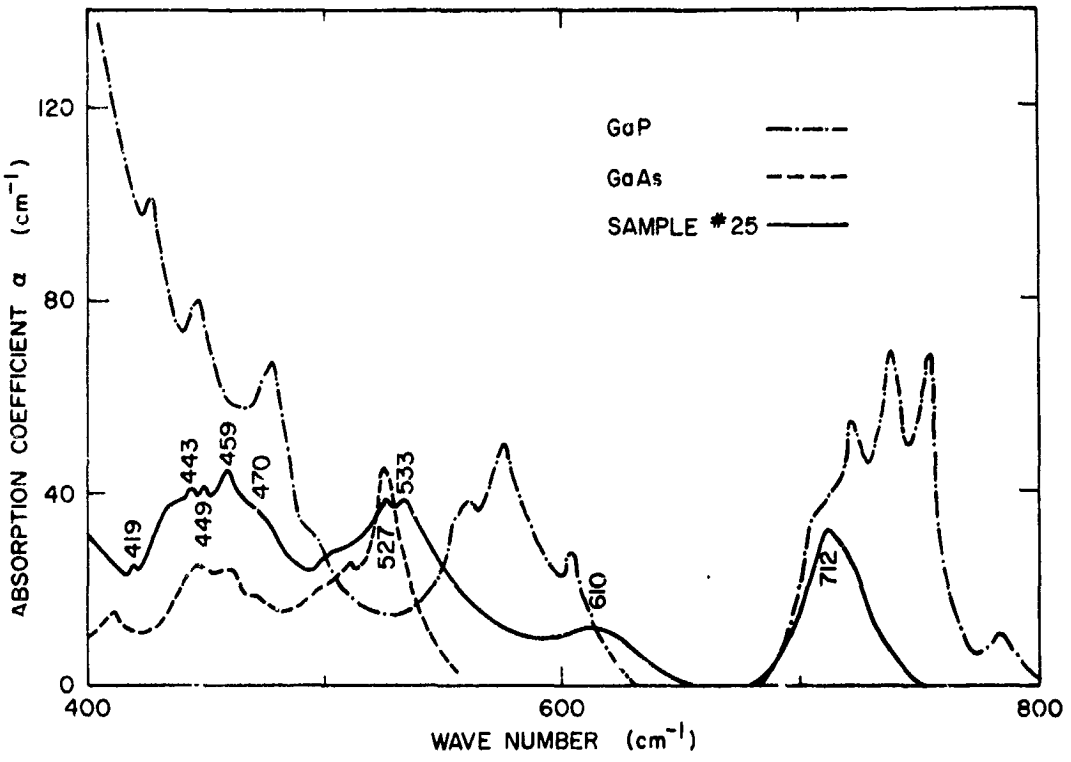

e. $GaAs_{0.65}P_{0.35}$

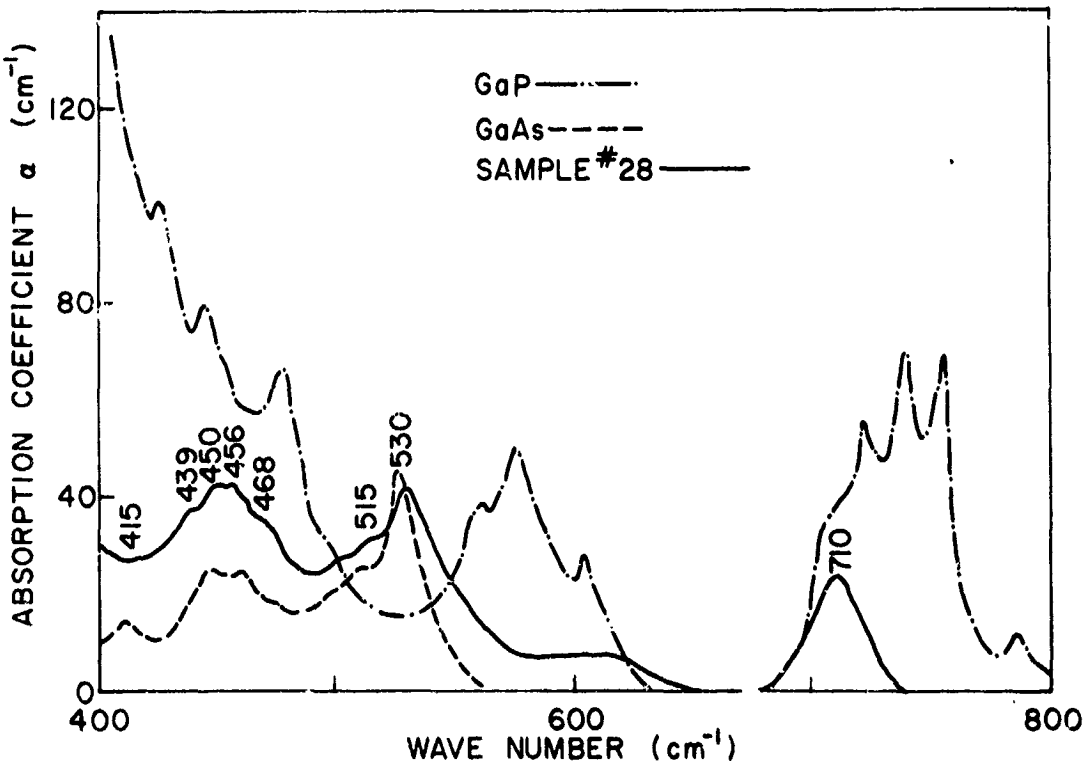

f. $GaAs_{0.823}P_{0.177}$

FIG. 15 (CONTINUED).

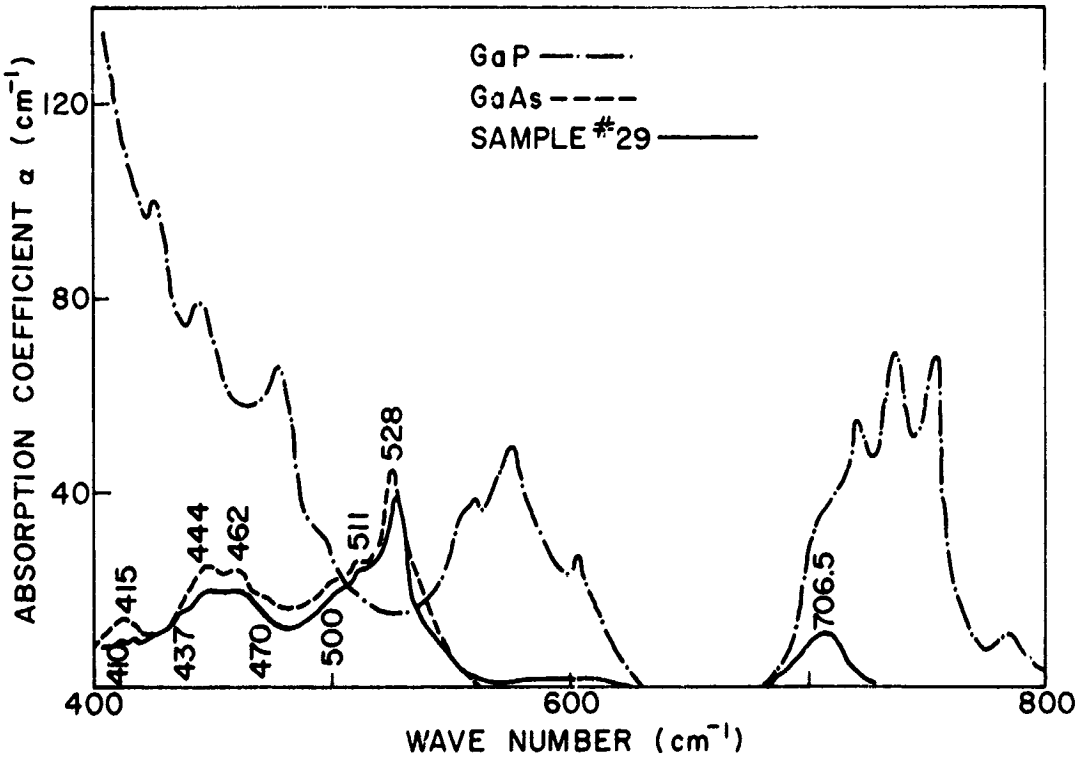

g. $GaAs_{0.946}P_{0.054}$

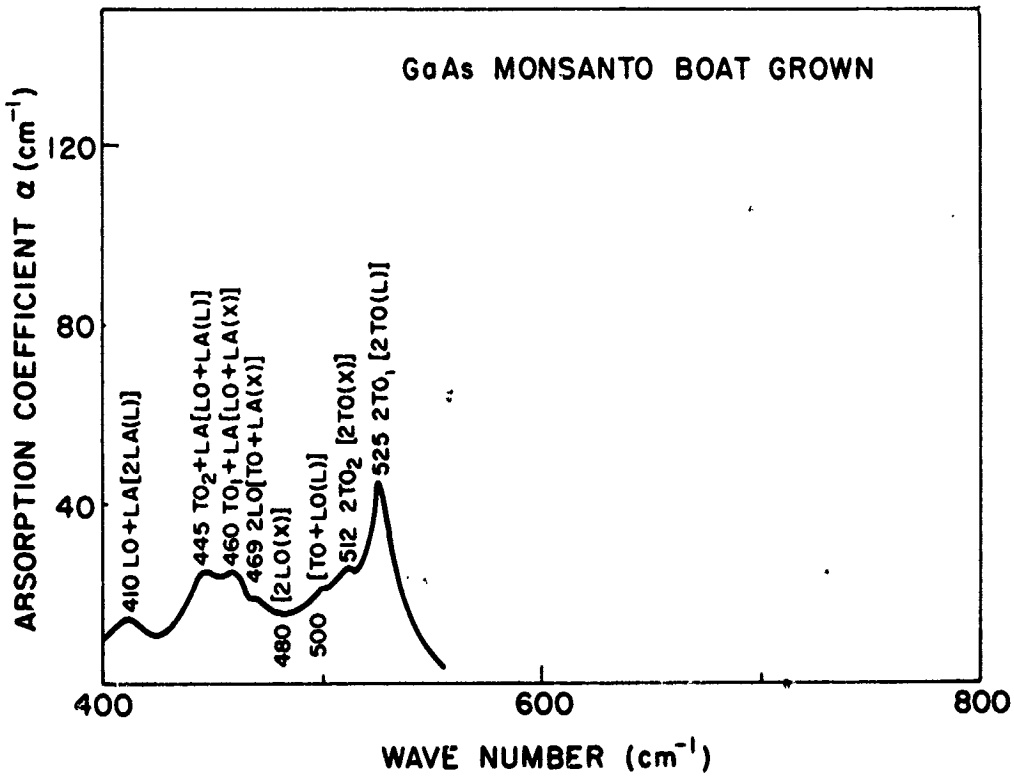

h. GaAs. Phonon assignment schemes by Cochran [Ref. 26] and Johnson [Ref. 21] are given, with the latter shown inside the brackets.

FIG. 15 (CONTINUED).

agreement between these schemes on a given material is poor; however, it is believed that Johnson's assignments are sounder because they have included consideration of the physical properties of crystal.

The sample of 5.4 percent phosphorus was subject to an annealing at 1169 ^{o}C for 72 hours. The purpose of this experiment was to investigate the effect of the diffusion of arsenic and phosphorus atoms within the lattice at an elevated temperature on the two-phonon absorption spectra. The experiment was carried out in a sealed evacuated ampoule with added arsenic and phosphorus to prevent the dissociation of the sample. No change in the two-phonon absorption spectra was observed. In particular, the shape and the position of the absorption peak at 706.5 cm^{-1} were unaffected by the annealing treatment. It is thus believed that the crystals grown at 800 ^{o}C by the epitaxial method do not contain gross inhomogeneities in the distributions of arsenic and phosphorus atoms within the lattice. The absorption spectra would be affected otherwise.

The major feature of the absorption spectra of $GaAs_xP_{1-x}$ is that it is possible to trace the energies of the two-phonon bands of GaAs and GaP in the alloy as a function of composition; this is shown in Fig. 16 where the assignments of phonons are indicated. In other words, a superposition of the two-phonon bands in the pure materials is observed in the alloy. Such a result is not too surprising since the phonons involved in these interactions are expected to be of very short wavelength in vibration and hence sensitive to the local distribution of arsenic and phosphorus atoms. The phenomenon of the superposition of bands in alloy can therefore be attributed to the microscopic clustering of either As or P atoms at the group V sites in the zinc blende structure due to statistical distribution. This will be discussed further in Chapter VI.

D. DISCUSSION

1. 604 cm^{-1} Band in GaP

A band at 604 cm^{-1} was observed by Kleinman and Spitzer [Ref. 23] in GaP which was grown by the reaction of gallium with phosphorus at an elevated temperature under a pressure of 20 atoms. This band was

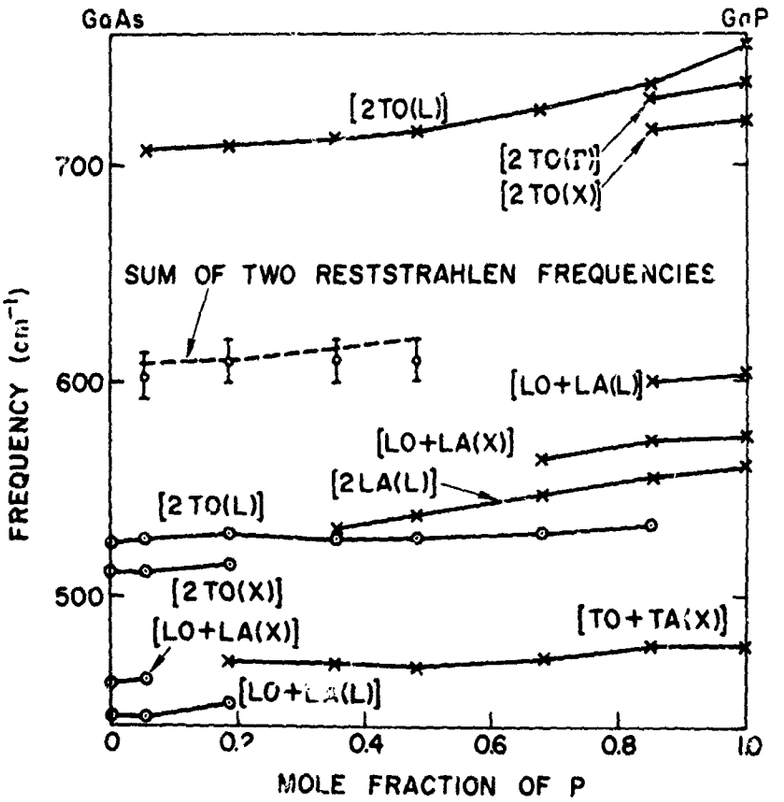

FIG. 16. TWO-PHONON BANDS OF $GaAs_xP_{1-x}$ AS A FUNCTION OF COMPOSITION. Johnson's assignment schemes for GaAs and GaP [Ref. 21] are given in brackets.

not included in their phonon assignment scheme and was attributed to the molecular vibrations of an unidentified impurity. In the present investigation the same band was observed in a sample which was grown epitaxially at 820 °C. In addition, a similar band was found at 600 cm^{-1} in an alloy of 85 percent phosphorus; the frequency shift of this band in the alloy agrees with that of the other bands of GaP as shown in Fig. 16. It is possible that the band at 604 cm^{-1} in GaP is intrinsic to GaP and is indeed one of the lattice two-phonon summation bands. Johnson's assignment has included this band as the [LO + LA(L)] mode. Such an assignment is therefore adequate.

2. Optical Modes of GaP

The superposition of GaAs and GaP bands in the alloy is most clearly indicated by the two-phonon bands of GaP near 700 cm^{-1}. These are the two-phonon summation bands of various optical phonons as indicated in Fig. 15a [Refs. 21, 23]. This group of bands continues to exist throughout the entire composition range, shifting toward smaller wave number as the phosphorus content decreases. The structure of the bands is maintained in the sample of 85 percent phosphorus; however, when the phosphorus content in the alloy is below 67.5 percent, the structure loses its detail and assumes the form of a broad band. The integrated absorption $\int \alpha d\lambda$ of these optical modes as a function of the mole fraction of phosphorus in the alloy is shown in Fig. 17 as a straight line through the origin. In other words, the photon-phonon interaction in this spectral region is contributed solely by the GaP-like phonons.

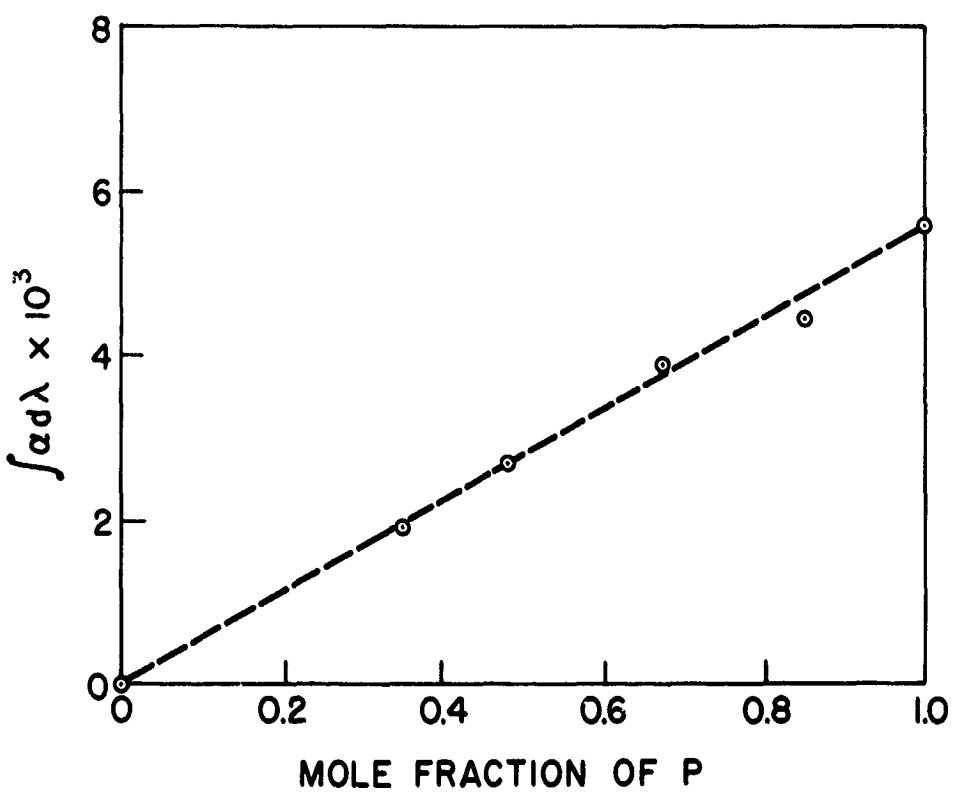

FIG. 17. INTEGRATED INTENSITY $\int \alpha d\lambda$ VS COMPOSITION OF $GaAs_xP_{1-x}$. (Spectral region of 660 to 800 cm^{-1}.)

The assignment scheme by Kleinman and Spitzer no longer holds in the 85-percent-phosphorus sample because the energy shifts of these bands in the alloy from the pure GaP values are such that the middle peak, TO+LO (731 cm^{-1}), no longer bisects the outer two peaks, 2TO and 2LO (738 and 716 cm^{-1}), on the wave number scale. On the other hand, Johnson's assignment still holds since the bands are designated as [2TO(L)] (738 cm^{-1}), [2TO(Γ)] (731 cm^{-1}), and [2TO(X)] (716 cm^{-1}).

3. "Summation" Band

In Chapter IV it was suggested that a band near 610 cm^{-1} might exist in the two-phonon absorption spectra of $GaAs_xP_{1-x}$ due to the simultaneous excitation of two Reststrahlen modes by the radiation. Such a band was indeed observed in the spectra shown in Figs. 15d to 15g in samples with arsenic content larger than 0.50. (This is the same composition region where reflectivity spectra show two maxima.) Its absorption strength is equivalent to that of a two-phonon process, and indeed decreases as the mole fraction of phosphorus decreases. This "summation" band arises from the interaction of radiation with both constituents simultaneously. However, the major part of the spectra of the alloy is due to a combination of interactions with the individual constituents.

4. Superposition of Bands and Phonon Energies

The superposition of bands of the pure materials in the alloy is most clearly indicated by the optical modes of GaP near 700 cm^{-1}, since this group of bands is located in the spectral region in which GaAs is completely transparent. It is noticed that a band at 706.5 cm^{-1} is distinctly detectable in the sample of only 5.4 percent phosphorus.

The superposition of bands is also observed in the energy shifts of the 525 cm^{-1} [2TO(L)] band of GaAs and the 560 cm^{-1} [2LA(L)] band of GaP. The fact that these bands are nearly at the same energy at a composition of 17.7 percent phosphorus is believed to be accidental since the nature of the bands is different as indicated by the phonon assignments. At a composition of 67.5 percent phosphorus, a plateau is formed on the spectra so that the bands are well separated and are of approximately the same intensity in absorption. At 85 percent phosphorus,

the GaP band becomes very dominant and has the shape of pure GaP, while the GaAs-like band forms a weak absorption peak at 534 cm^{-1}.

As indicated in Fig. 16, the two-phonon bands of GaP shift toward smaller wave number, while those of GaAs shift toward larger wave number as a small percentage of the minority constituent is added. Some of the two-phonon bands cannot be traced from the spectra of the alloy; this is particularly true for the bands of GaAs since the intensity of the GaP bands is inherently stronger than that of the GaAs bands. On the other hand, a number of the GaP bands appear in a spectral region in which GaAs is completely transparent and therefore they are easy to be traced. The phonon energies are given in Table 3 and are plotted in Fig. 18 as a function of composition. The assignment schemes are those of Johnson [Ref. 21].

TABLE 3. PHONON ENERGIES OF $GaAs_xP_{1-x}$ OBTAINED FROM THE ABSORPTION SPECTRA

Phonon		Phonon Energies (cm^{-1})							
		Composition (% P)							
		100 (GaP)	85	67.5	48	35	17.7	5.4	0 (GaAs)
L	TO	377.5	369	363	358	356	355	353.3	
	LO	329.5	321.5						
	LA	280	278.5	274	269.5	266.5	265		
	TA	68.5	71	77	82	84	84	84	
X	TO	360.5	358						
	LO	309	300						
	LA	265	273						
	TA	117.5	120						
L	TO		267	265	263.5	263.5	265	264	262.5
	LO							238	237.5
	LA							206	206.5
X	TO						257.5	255.5	256
	LO							240	240
	LA							222	220

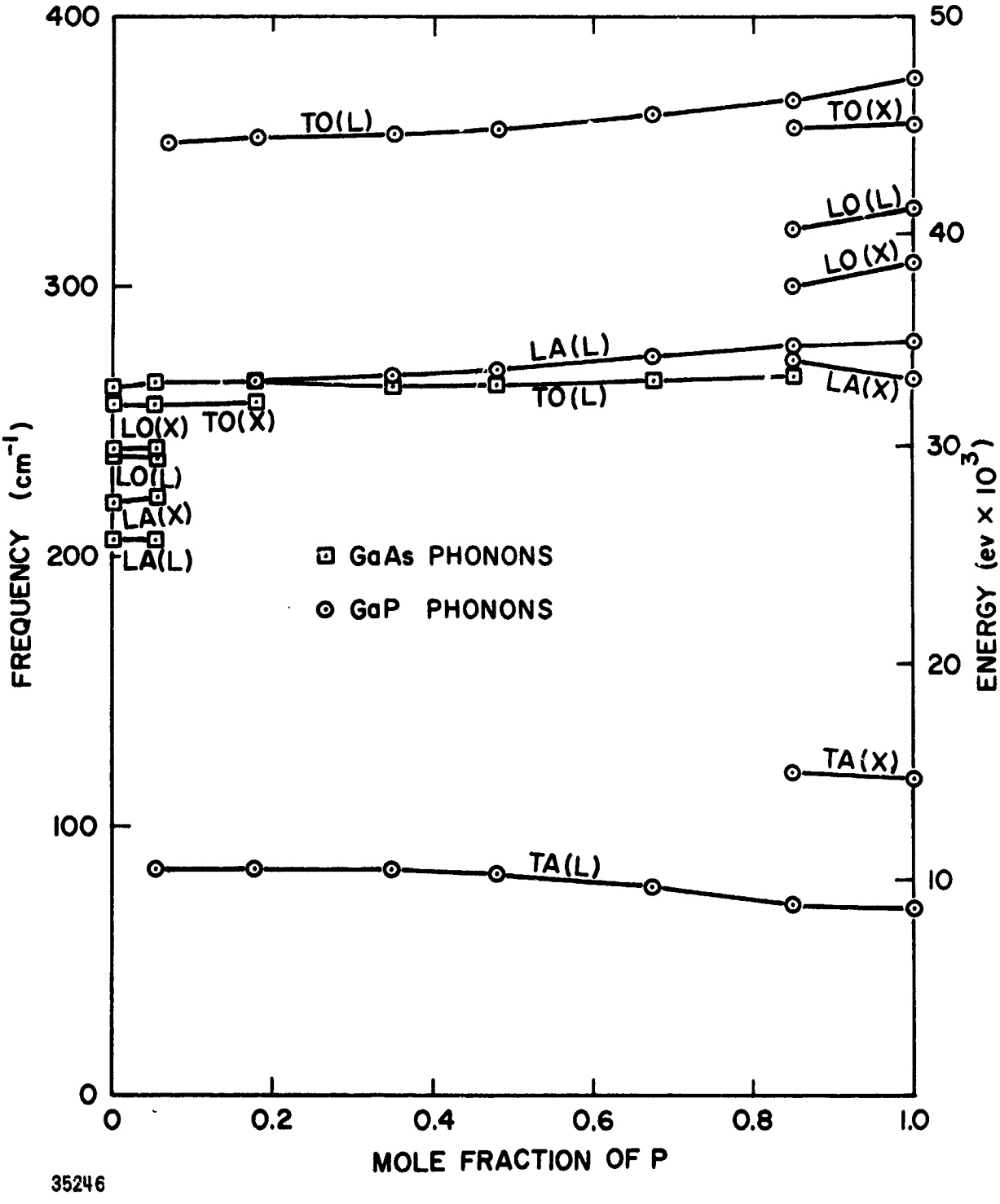

FIG. 18. PHONON ENERGIES IN $GaAs_xP_{1-x}$ OBTAINED FROM THE ABSORPTION SPECTRA.

VI. INTERPRETATION OF THE SPECTRA

A. INTRODUCTION

In the course of studying the nature of the electronic properties in the binary alloys of semiconductors, continuous and single-valued variations as a function of the composition have been observed by a number of workers. Specific examples are the shifts in the energy gaps of $GaAs_xP_{1-x}$ [Ref. 27], Si-Ge alloys [Ref. 28], and other thermodynamically mixable alloys. Similar variation has also been observed in the $GaAs_xP_{1-x}$ band structure within a few electron volts of the band gap [Ref. 29]. The variation of the lattice constant in the alloy is of the same nature [Ref. 7]. However, the experimental results of this work, as well as those on Si-Ge alloys by Braunstein [Ref. 3], indicate that the vibrational modes of each constituent exist independently and do not form a continuous and single-valued variation for a particular mode. Although it was mentioned in Chapter III that the most powerful method for studying the phonon spectra is by inelastic thermal neutron scattering, it is through the interaction of these modes with the infrared radiation that many important findings are revealed.

The phonon spectrum of a disordered system is sensitive to the distribution of different species of atoms. In the case of $GaAs_xP_{1-x}$, the gallium atoms are always located in one of the two face-centered cubic sublattices and hence no disorder is involved in this sublattice. The arsenic and phosphorus atoms are located in the other sublattice. It is important to emphasize that the following experimental findings show that the distribution of the group V atoms is macroscopically homogeneous:

1. A well-defined energy gap as shown by the band-edge absorption measurement.
2. A well-defined lattice constant as shown by the X-ray measurement.
3. The invariance of the two-phonon absorption bands to the annealing treatment.
4. A well-defined frequency shift of the Reststrahlen bands in the alloy.

In addition, recent results on the Gunn effect on $GaAs_xP_{1-x}$ [Ref. 30] show that the transport properties of free carriers in these crystals are similar to those in the ordered crystals such as GaAs. Any inhomogeneities in the distribution of the group V atoms in the alloy are thus expected to be microscopic, involving at most a few unit cells in dimension. The experimental results should be interpreted in the light of these considerations.

B. QUALITATIVE INTERPRETATIONS

The findings are similar in both the Reststrahlen band and the two-phonon band experiments on $GaAs_xP_{1-x}$ in that the modes of each constituent exist independently in the alloy. The phonons involved in the two-phonon process are located near the boundaries of the Brillouin zone. The large wave vectors of these phonons indicate that their vibrational wavelengths are extremely short and are of the order of one lattice constant. Although it was emphasized in Section A that there are no gross inhomogeneities in the distribution of the group V elements in the alloyed crystals, microscopic clustering of the minority constituent can still exist through the random distribution of constituent atoms in the lattice. The clustering size of only a few unit cells is large enough to support the vibrational modes investigated in the two-phonon absorption spectra. It should be recognized that the interactions of radiation are not limited to just those with the phonons of the individual constituent. The identification of the "summation" band near 610 cm^{-1}, described in Section V.D, shows that the interaction between As and P atoms is significant in the lattice. This interaction supports the concept that the clustering of the minority constituent in the alloy is only microscopic and is a result of the statistical fluctuation in the atomic distribution.

So far as the TO phonons near the zone center are concerned, their wavelengths are much larger than a lattice constant. This is one of the properties that make the first-order photon-phonon interaction possible. However, the vibrational frequency, and hence the phonon energy, is determined by the relative motion of one face-centered cubic sublattice against the other in crystals having diamond or zinc blende structure.

The atomic motion in one unit cell is typical of the whole crystal, and therefore can be considered to be localized; this is why the TO branch is nearly flat in the phonon spectrum of GaAs. It is thus not surprising to have detected two resonant modes in the reflectivity spectra of the alloys. These represent, in the first-order approximation, the vibrational modes of randomly distributed P and As atoms against ordered Ga atoms in the lattice.

C. GRÜNEISEN RELATION

A well-defined mean lattice constant was found for each of the alloyed crystals to an accuracy of ±0.0005 Å. The variation of lattice constant vs composition of the alloy follows Vegard's law [Ref. 7]. In the case of GaAs, the lattice is contracted when a portion of the As atoms is replaced randomly by P atoms. If a small portion of As atoms is replaced, the lattice is mainly occupied by the Ga-As bonds. Therefore, it is reasonable to assume that the phonons of GaAs in $GaAs_xP_{1-x}$ with $x \cong 1$ should behave like the same phonons in the pure GaAs under compression. By the same token, the phonons of GaP in $GaAs_xP_{1-x}$ with $x \cong 0$ should behave like the same phonons in the pure GaP under tension. Thus the energies of these phonons should, to a first-order approximation, obey Grüneisen's law [Ref. 31] which states that

$$\alpha_v = \gamma_{Gr} \frac{KC_V}{V} \quad , \tag{6.1}$$

where γ_{Gr} = the Grüneisen constant given by the relation

$$\gamma_{Gr} = - \frac{\Delta\omega_p/\omega_p}{\Delta V/V} \tag{6.2}$$

α_v = volume expansion coefficient

K = compressibility

V = volume of one gram atom

C_V = specific heat per gram atom at constant volume

ω_p = phonon frequency in the solid

In the case of GaP [Refs. 32, 33],

$$\alpha_v = 15.9 \times 10^{-6} \text{ deg}^{-1}$$
$$V = 4.13^{-1} \text{ cm}^3 \text{ gm}^{-1}$$
$$C_V = 0.124 \text{ cal gm}^{-1} \text{ deg}^{-1}$$
$$K = 0.77 \times 10^{-12} \text{ dyne cm}^{-2}$$

From Eq. (6.1) it is calculated that $\gamma_{Gr} = 0.97$, and from Eq. (6.2)

$$\frac{\Delta\omega_p}{\omega_p} = -0.97 \frac{\Delta V}{V} = -0.108(1-x) \qquad \text{for } x \cong 0 . \qquad (6.3)$$

In the case of GaAs [Ref. 33],

$$\alpha_v = 17.1 \times 10^{-6} \text{ deg}^{-1}$$
$$V = 5.32^{-1} \text{ cm}^3 \text{ gm}^{-1}$$
$$C_V = 0.086 \text{ cal gm}^{-1} \text{ deg}^{-1}$$
$$K = 1.34 \times 10^{-12} \text{ dyne cm}^{-2}$$

so that $\gamma_{Gr} = 0.675$ and

$$\frac{\Delta\omega_p}{\omega_p} = 0.675 \frac{\Delta V}{V} = 0.073x \qquad \text{for } x \cong 1 . \qquad (6.4)$$

The value of γ_{Gr} given here is the average value over all the phonon modes in the crystal according to the following relation [Ref. 34]:

$$\gamma_{Gr} = \frac{\sum_{j=1}^{3N} \gamma_j C_{Vj}}{\sum_{j=1}^{3N} C_{Vj}} , \qquad (6.5)$$

where γ_j and C_{Vj} are respectively the Grüneisen constant of the j^{th} mode and the heat capacity of the same mode at the temperature of observation. The observed values of the Grüneisen constants for various modes are given in Table 4. It is noticed that the γ_j of the TO(Γ) and TO(L) modes of both GaP and GaAs agree well with the values given by Eqs. (6.3) and (6.4). However, the energy shift of the TA(L), TA(X), and LA(L) modes of GaP is opposite to the relation given in Eq. (6.3); this indicates that a negative Grüneisen constant is called for. Negative Grüneisen constants of the acoustical modes for Ge were observed by Fritzsche and Teimann [Ref. 35]; those for Si-Ge alloys were observed by Braunstein [Ref. 3] and were later pointed out by

TABLE 4. GRÜNEISEN CONSTANTS FOR PHONONS IN GaP AND GaAs

Phonon	γ_j[GaP γ_{Gr} = 0.97]	γ_j[GaAs γ_{Gr} = 0.675]
Γ TO	0.82	0.20
L TO	1.35	0.40
LO	1.45	0.30
LA	0.32	0
TA	-2.20	
X TO	0.25	0.30
LO	1.75	0
LA	-1.80	0
TA	-1.27	

Daniels [Ref. 34]. The similarity of the frequency variation of the acoustical modes with respect to the change in lattice constant between the homopolar and the III-V compound semiconductors is indeed reasonable [Ref. 34].

It should be pointed out that the Grüneisen relation is applied to the majority constituents only at the extreme values of x. Interactions between As and P atoms are expected to be significant in treating the general behavior of these phonons over the entire range of composition.

D. RESTSTRAHLEN FREQUENCIES

In this section the frequencies of the TO(Γ) phonons in $GaAs_xP_{1-x}$ are calculated over the entire range of composition. These particular modes are chosen because the atomic motions are known to be the vibrations of the randomly distributed As and P atoms in one face-centered cubic sublattice against the Ga atoms in the other sublattice. Furthermore, since the wavelength of radiation with which these phonons interact is much larger than the dimension of the statistical fluctuation in the distribution of the constituent atoms, average potentials can then be assigned to these atoms. The equations of motion for the three species of atoms in the lattice, under a linear-crystal approximation, are given as follows:

$$m_a\ddot{u}_a = -\xi(u_a-u_c) - x\eta(u_a-u_b) \tag{6.6}$$

$$m_b\ddot{u}_b = -\zeta(u_b-u_c) - (1-x)\eta(u_b-u_a) \tag{6.7}$$

$$m_c\ddot{u}_c = -x\zeta(u_c-u_b) - (1-x)\xi(u_c-u_a) , \tag{6.8}$$

where the subscripts a, b, and c represent P, As, and Ga atoms respectively, the u_i are the displacements, the m_i are the masses, x is the mole fraction of As, ξ and ζ are the force constants between Ga and P and between Ga and As as first nearest neighbors, and η is the force constant between As and P as second nearest neighbors.

This is a virtual crystal model in that each P (or As) atom is given a probability of x (or 1-x) for having As (or P) as its second nearest neighbor, and in that each Ga atom is given probabilities x and 1-x for having As and P as its first nearest neighbors respectively. The force constants ξ and ζ are used to explain the existence of two modes in the reflectivity spectra, and the force constant η is used to fit the frequency shifts of these modes in the alloy. In addition, let these force constants be represented by F; then

$$F = F_o(1-\theta x) \ , \tag{6.9}$$

where θ is determined by the Grüneisen relation; this corresponds to the change in the binding strength as a result of the change in lattice constant from that of GaP (5.450 Å) to that of GaAs (5.653 Å). From Eq. (6.3) θ is found to be 0.216 for pure GaP and this value is used in the calculations.

The center of gravity of the entire system remains stationary; this is indicated by the sum of atomic motions in the following equation:

$$m_c\ddot{u}_c + xm_b\ddot{u}_b + (1-x)m_a\ddot{u}_a = 0 \ . \tag{6.10}$$

In the case of sinusoidal vibration, the frequency ω is determined by the following equation:

$$\begin{vmatrix} m_a\omega^2 - \xi - x\eta & x\eta & \xi \\ (1-x)\eta & m_b\omega^2 - \zeta - (1-x)\eta & \zeta \\ (1-x)\xi & x\zeta & m_c\omega^2 - (1-x)\xi - x\zeta \end{vmatrix} = 0 \ . \tag{6.11}$$

One trivial solution is $\omega^2 = 0$, which is equivalent to the expression given by Eq. (6.10). The remaining part of Eq. (6.11) is a quadratic equation in ω^2. The following solutions are obtained in the limits of $x = 0$ and $x = 1$:

For $x = 0$,

$$\omega^2 = \begin{cases} \dfrac{\xi_o}{m_a}\left(1 + \dfrac{m_a}{m_c}\right) , & (6.12a) \\ \dfrac{\zeta_o + \eta_o}{m_b} . & (6.12b) \end{cases}$$

For $x = 1$,

$$\omega^2 = \begin{cases} \left(\dfrac{\xi_o + \eta_o}{m_a}\right)(1-\theta) , & (6.13a) \\ \dfrac{\zeta_o}{m_b}\left(1 + \dfrac{m_b}{m_c}\right)(1-\theta) . & (6.13b) \end{cases}$$

Frequencies given by Eqs. (6.12a) and (6.13b) are the Reststrahlen frequencies of GaP and GaAs respectively; those given by Eqs. (6.12b) and (6.13a) are the vibrational frequencies of As and P atoms in the host lattices of GaP and GaAs respectively. The measured data in Table 2 can be extrapolated to obtain ω in Eq. (6.13a). Frequencies corresponding to Eqs. (6.12a), (6.13a), and (6.13b) are used to determine ξ_o, ζ_o, and η_o. The resulting values in gm cm^{-2} are

$$\xi_o = 2.86 \times 10^6 ,$$

$$\zeta_o = 3.32 \times 10^6 ,$$

$$\eta_o = 1.72 \times 10^6 .$$

The units used here are molegrams for the masses and cm^{-1} for the frequency. The above force constants are used in Eqs. (6.9) and (6.11) to obtain the frequencies of vibration as a function of x. The calculated values are given in Table 5 and are plotted in Fig. 19. The agreement between the calculated and the measured frequencies is within 2 percent, which is exceedingly good.

TABLE 5. CALCULATED VALUES OF RESTSTRAHLEN FREQUENCIES IN $GaAs_xP_{1-x}$ AS A FUNCTION OF COMPOSITION

Composition (% P)	ω_{TO} of GaP (cm^{-1})	ω_{TO} of GaAs (cm^{-1})
0	340	268
20	345	268
40	349	268
60	354	266.5
80	360	264
100	366	260

The model proposed here, though based on simple first principles, is physically sound since it takes into account three important points:

1. The fact that the wavelength of the $TO(\Gamma)$ phonons is large in comparison with the dimension of the statistical fluctuation in the atomic distribution.
2. The effect of change in lattice constant on the binding forces between nuclei.
3. The interaction of the As and P atoms as second nearest neighbors.

The force constant η at the extreme values of x is shared by 12 second nearest neighbors; in other words, it is shared by 12 As-P bonds. The resulting force constant per bond is much smaller than those equivalent force constants involving the first nearest neighbors (ξ and ζ are shared by four neighbors). The relative strength is 1:5, which is further evidence that the model considered here is physically sound.

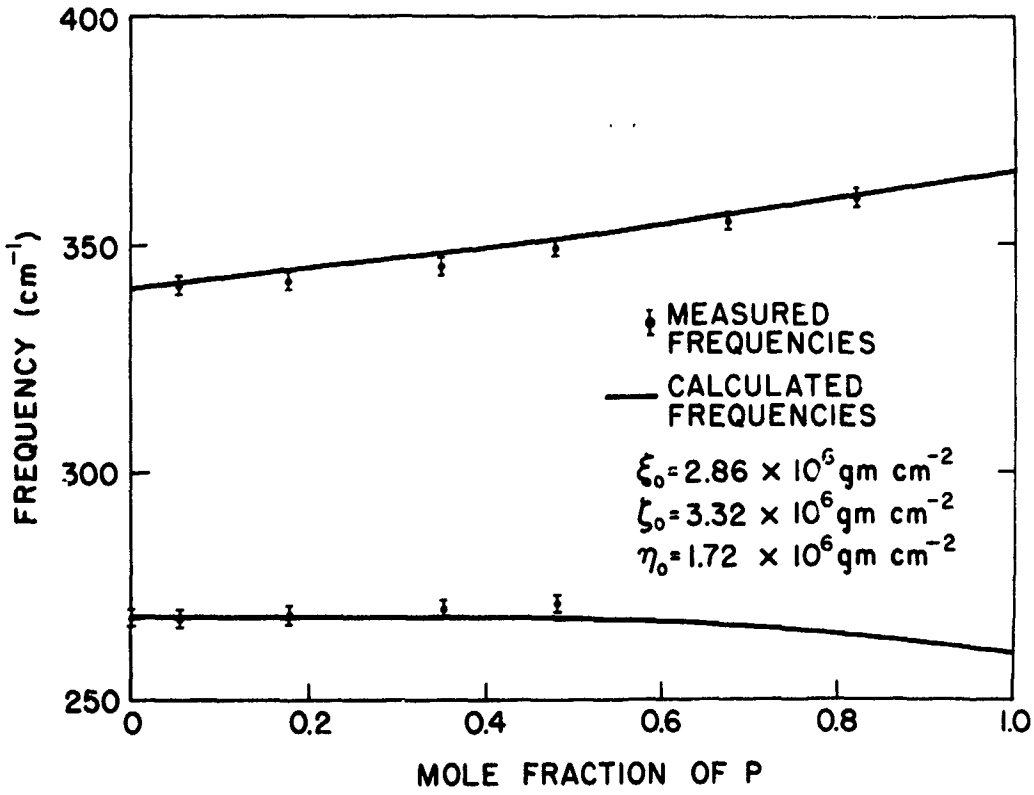

FIG. 19. CALCULATED RESTSTRAHLEN FREQUENCIES IN $GaAs_xP_{1-x}$.

E. SUMMARY

A great deal of fundamental knowledge--not previously available--has been obtained which relates to the phonon spectra of $GaAs_xP_{1-x}$ and which can be applied to disordered systems in general. The spectra have been found to have the following properties:

1. Phonons characteristic of both GaAs and GaP exist near and at the boundaries of the Brillouin zone. Their existence is due to the presence of microscopic clustering of the minority constituent arising from statistical fluctuation in the atomic distribution.
2. TO phonons characteristic of both GaAs and GaP also exist at the center of the Brillouin zone. Their presence is chiefly due to the vibrations of As and P atoms against the Ga atoms as first nearest neighbors. A theoretical model has been proposed to explain the experimental results and good agreement was obtained. The interaction between As and P atoms as second nearest neighbors in the alloy was specifically considered.

The Grüneisen relation was also applied to the phonon energies observed in the alloy; and the results can serve as a guide to the problem of pressure dependence of phonon frequencies in GaAs and GaP.

VII. CONCLUDING REMARKS

Although the alloy system of $GaAs_xP_{1-x}$ has been specifically studied in this work, it is believed that the results obtained are typical of many semiconductor alloys. On this basis the present work can serve as a check on more detailed theories involving three-dimensional disorder problems which may be proposed in the future.

The results obtained in this study are summarized in the following paragraphs.

1. Single crystals of $GaAs_xP_{1-x}$ were successfully grown on GaAs substrates in an open-tube epitaxial vapor growth system. The source materials were Ga, PCl_3, and $AsCl_3$; and the chemical reactions took place in a hydrogen atmosphere. The composition of the grown crystal was found to depend entirely on the mole ratio of PCl_3 to $AsCl_3$ carried into the reaction tube by the hydrogen flow; thus the process developed in this work is extremely reproducible. Crystals grown by this process were found to be low in carrier concentration, consistently below 10^{15} cm^{-3} (electrons) at room temperature, and to be free of any gross inhomogeneities in the distribution of the constituent atoms.

2. Reflectivity spectra of $GaAs_xP_{1-x}$ were taken at 300 ^oK in the region of 220 to 500 cm^{-1} (0.027 to 0.062 ev). Two Reststrahlen modes were detected in the alloy such that their frequencies are close to those of the TO(Γ) phonons in GaAs and GaP respectively. The absence of the GaAs-like mode in the GaP-rich samples is in good agreement with the theory given by Dawber and Elliott [Ref. 25]. Absorption spectra in $GaAs_xP_{1-x}$ were taken at 300 ^oK in the region of 400 to 800 cm^{-1} (0.05 to 0.10 ev). A number of two-phonon absorption bands were observed in these spectra. A superposition of the bands characteristic of GaAs and GaP was observed in the alloy. This result is similar to that obtained by Braunstein [Ref. 3] on Si-Ge alloys. The present experimental results supported Johnson's assignment schemes for the bands in GaAs and GaP [Ref. 18], and these schemes were therefore used to calculate the energies of several GaAs and GaP phonons in the alloy as a function of composition. An absorption band was found near 610 cm^{-1} in the GaAs-rich samples and it was identified as the "summation" band

of the two TO(Γ) phonons in the alloy. The existence of such a band suggests that the interaction between As and P atoms in the lattice is significant.

3. The superposition of bands characteristic of GaAs and GaP in the two-phonon absorption spectra of $GaAs_xP_{1-x}$ is attributed to the presence of microscopic clustering of the minority constituent in the alloy arising from statistical fluctuation in the random atomic distribution. This explanation is valid since phonons involved in these interactions have extremely short vibrational wavelengths. The Reststrahlen band spectra in the alloys are explained by a model in which the presence of two resonant modes is attributed to the vibrations of both As and P atoms against Ga atoms in the lattice as the first nearest neighbors, and the frequency shifts of these modes in the alloy are fitted by a parameter representing the interactions between As and P atoms as second nearest neighbors. This is a virtual crystal model because average parabolic potentials are given to the three species of atoms in the lattice. This model is justified since (1) the distribution of these atoms in the lattice is free of gross inhomogeneity, and (2) the long wavelength nature of the TO(Γ) phonons is involved in their interactions with the radiation. Good agreement is obtained between the data and the theoretical calculations. The model thus demonstrates that it is incorrect to interpret the results of this work by assuming gross inhomogeneities in the distribution of the constituent atoms in the alloy.

APPENDIX A. DISPERSION THEORY

1. Definition of the Optical Constants

Optical constants are used in treating the interactions between the electromagnetic radiation and matter. These constants are defined by means of Maxwell's equations:

$$\left.\begin{aligned} \nabla \times \vec{H} &= \epsilon \frac{\partial \vec{E}}{\partial t} + \sigma \vec{E} \\ \nabla \times \vec{E} &= -\mu \frac{\partial \vec{H}}{\partial t} \\ \nabla \cdot \vec{H} &= 0 \\ \nabla \cdot \vec{E} &= 0 \end{aligned}\right\}, \qquad (A.1)$$

where $\vec{E}$ and $\vec{H}$ are the electric and magnetic field vectors, ϵ is the dielectric constant, μ is the permeability, and σ is the conductivity of the material. Both ϵ and σ are frequency dependent, and $\mu = \mu_{vac}$ for most materials of interest. Equation (A.1) can be manipulated to give

$$\nabla^2 \vec{E} - \sigma\mu \frac{\partial \vec{E}}{\partial t} - \epsilon\mu \frac{\partial^2 \vec{E}}{\partial t^2} = 0 \ . \qquad (A.2)$$

The time-harmonic solution of Eq. (A.2) can be written as a plane wave

$$\vec{E} = \vec{x}_o E_o \exp\left[i\omega\left(t - \frac{\bar{n}z}{c}\right)\right] \ , \qquad (A.3)$$

where $\bar{n}$ is defined as the complex index of refraction. The index of refraction n and the extinction coefficient k satisfy the relation $\bar{n} = n - ik$. Substituting Eq. (A.3) into (A.2) gives

$$\bar{n}^2 = c^2\mu\epsilon - ic^2\frac{\sigma\mu}{\omega} = \frac{\epsilon}{\epsilon_o} - i\frac{\sigma}{\epsilon_o\omega} = \bar{\epsilon}(\omega)$$

$$\bar{n} = \sqrt{\bar{\epsilon}(\omega)} \quad . \tag{A.4}$$

Notice that the newly defined $\bar{\epsilon}(\omega)$ is complex.

The reflectivity of matter with normal incidence can be shown to be

$$R = \left|\frac{\bar{n}-1}{\bar{n}+1}\right|^2 = \frac{(n-1)^2 + k^2}{(n+1)^2 + k^2} \quad . \tag{A.5}$$

2. Ionic Polarization

The Reststrahlen band in the reflectivity spectra of an ionic crystal is due to the excitation of the resonance mode in the crystal by radiation; such a mode can be described by the relative motion of the cations and anions in the crystal. We shall consider a simple diatomic chain composed of atoms of mass m and charge $-e$ and atoms of mass M and charge $+e$. The equation of motion of such a system can be written as

$$M_R\ddot{w} = -2\beta w + e\vec{E} \quad , \tag{A.6}$$

where w is the relative displacement of the ions, β is the force constant between the ions, and M_R is the reduced mass of the ion pair. The time-harmonic solution is

$$w = \frac{eE_o}{M_R}\frac{1}{\omega_0^2 - \omega^2} \tag{A.7}$$

where $\omega_0^2 = 2\beta/M_R$. The process described here is for one-dimensional systems, but it can be regarded as a good approximation to three-dimensional ionic crystals.

The total ionic polarization from such a vibration is

$$P = \frac{ew}{\Omega} ,$$

where Ω is the volume per molecule. In this simple treatment the local field in the solid is regarded to be the applied field. The dielectric constant is found to be

$$\epsilon(\omega) = \epsilon_o \left(1 + \frac{4\pi P}{E_{loc}}\right) . \qquad (A.8)$$

After combining various constants, Eq. (A.8) can be rewritten as

$$\epsilon(\omega) = \epsilon_\infty + \frac{\epsilon_o - \epsilon_\infty}{1 - (\omega/\omega_0)^2} , \qquad (A.9)$$

where ϵ_o is the static dielectric constant and ϵ_∞ is the high-frequency dielectric constant.

The dielectric constant given in Eq. (A.9) is real, since no dissipative force is included in the treatment. This force is introduced in the following modification to Eq. (A.6),

$$M_R \ddot{w} = -2\beta w - \gamma \dot{w} + e\vec{E} , \qquad (A.10)$$

where γ is a positive constant with the dimension of frequency; the additional term represents a force always opposed to the motion. Equation (A.9) is then modified to be

$$\bar{\epsilon}(\omega) = \epsilon_\infty + \frac{\epsilon_o - \epsilon_\infty}{1 - (\omega/\omega_0)^2 - i(\omega/\omega_0)(\gamma/\omega_0)} . \qquad (A.11)$$

3. Reflectivity Spectra

From Eqs. (A.4), (A.5), and (A.11) it is possible to plot n, k, and R as a function of frequency once ϵ_o, ϵ_∞, and γ are known. The shape of the reflectivity curve is of interest here and a typical result is given in Fig. 20, taken from a paper by Picus et al [Ref. 36].

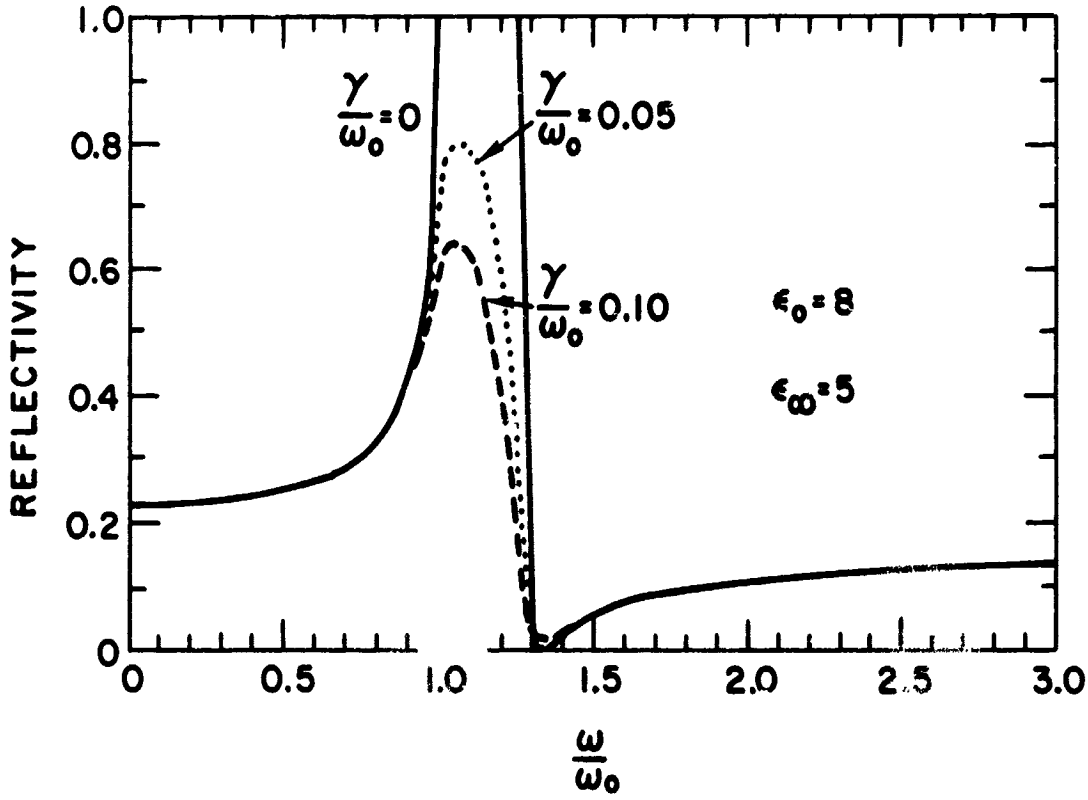

35232

FIG. 20. THEORETICAL REFLECTIVITY CURVES FOR DIFFERENT DISSIPATIVE FORCES. [From Picus et al, Ref. 36.]

The reflectivity curve for $\gamma = 0$ can be discussed in four separate regions of frequency:

1. In the region $0 < \omega < \omega_0$, R increases from its low-frequency value, $[(\sqrt{\epsilon_o} - 1)/(\sqrt{\epsilon_o} + 1)]^2$, up to 1.
2. In the region $\omega_0 < \omega < \omega_1$, with $\omega_1 = \sqrt{\epsilon_o/\epsilon_\infty}\ \omega_0$, $\epsilon(\omega)$ is negative; therefore $\bar{n}$ is imaginary and R = 1.

3. Above ω_1, R decreases sharply to zero at a frequency ω_m such that $\epsilon(\omega_m) = 1$ or $\bar{n} = 1$. The value of ω_m is found to be $\omega_0 [1 + (\epsilon_\infty - \epsilon_o)/(\epsilon_\infty - 1)]^2$.

4. Beyond ω_m, R increases from zero to its high-frequency limit of $[(\sqrt{\epsilon_\infty} - 1)/(\sqrt{\epsilon_\infty} + 1)]^2$.

In the case $\gamma \neq 0$ and $\gamma/\omega_0 \ll 1$, the major influence on the reflectivity spectra will be in the region of the maximum as shown in Fig. 20. It can also be shown by Eqs. (A.4) and (A.11) that the maximum of the extinction coefficient k occurs at $\omega = \omega_0$; in other words, the strength of absorption is the strongest at the resonant frequency.

To conclude, it is possible to explain the shape of the reflectivity spectra from dispersion theory. The resonant frequency is located at ω_0 as shown in Fig. 20.

REFERENCES

1. P. Dean, Proc. Roy. Soc. (London), Ser. A, 254, 1960, p. 507.

2. Von F. Oswald, Z. Naturforsch., 14a, 1959, p. 374.

3. R. Braunstein, Phys. Rev., 130, 1963, p. 879.

4. J. F. Gibbons and P. C. Prehn, "Epitaxial Vapor Growth of III-V Compounds," Rept. SEL-63-105 (TR No. 4711-1), Stanford Electronics Laboratories, Stanford, Calif., Oct 1963.

5. H. C. Gatos and M. C. Lavine, "Chemical Behavior of Semiconductors: Etching Characteristics," Technical Report No. 293, Lincoln Laboratory, MIT, Jan 1963, p. 39.

6. Handbook of Chemistry and Physics, 40th ed., edited by C. D. Hodgman, Chemical Rubber Publishing Co., Cleveland, 1958, pp. 2335 and 2345.

7. R. A. Pizzarello, J. Electrochem. Soc., 109, 1962, p. 226.

8. R. A. Swalin, Thermodynamics of Solids, John Wiley & Sons, New York, 1962, p. 100.

9. C. Hilsum and A. C. Rose-Innes, Semiconducting III-V Compounds, Pergamon Press, New York, 1961, p. 13.

10. X-ray Powder Data File, Card No. 5-0565, American Society for Testing and Materials, Philadelphia, 1961.

11. R. A. Smith, Semiconductors, Cambridge University Press, London, 1961, p. 204.

12. W. G. Spitzer et al, J. Phys. Chem. Solids, 11, 1959, p. 339; and R. Eden, "Quarterly Research Review No. 9," Rept. SU-SEL-64-073, Stanford Electronics Laboratories, Stanford, Calif., 1 Apr through 30 Jun 1964, p. 11-17.

13. W. G. Spitzer and H. Y. Fan, Phys. Rev., 106, 1957, p. 882.

14. D. H. Loescher and M. Shyam, Stanford University, private communication.

15. F. A. Johnson and W. Cochran, Conf. on Semicond. Physics, Exeter, England, 1962, p. 498.

16. L. I. Schiff, Quantum Mechanics, 2d ed., McGraw-Hill Book Company, New York, 1955, p. 252.

17. S. Iwasa, I. Balslev, and E. Burstein, Conf. on Semicond. Phys., Dunod, France, 1964, p. 1077.

18. M. Born and K. Huang, Dynamical Theory of Crystal Lattices, Oxford University Press, London, 1962, p. 82.

19. M. Lax and E. Burstein, Phys. Rev., 97, 1955, p. 39.

20. D. A. Kleinman, Phys. Rev., 118, 1960, p. 118.

21. F. A. Johnson, Progress in Semiconductors, 9, Temple Press, London, 1965.

22. T. S. Moss, Optical Properties of Semiconductors, Butterworths Scientific Publications, London, 1959, pp. 6 and 13.

23. D. A. Kleinman and W. G. Spitzer, Phys. Rev., 118, 1960, p. 110.

24. R. F. Potter and D. L. Stierwalt, Conf. on Semicond. Phys., Dunod, France, 1964, p. 1111.

25. P. G. Dawber and R. J. Elliott, Proc. Roy. Soc. (London), Ser. A., 273, 1963, p. 222.

26. W. Cochran et al, J. Appl. Phys. Suppl., 32, 1961, p. 2102.

27. W. G. Spitzer and C. A. Mead, Phys. Rev., 133, 1964, p. A872.

28. E. R. Johnson and S. M. Christian, Phys. Rev., 95, 1954, p. 560.

29. E. Williams, Texas Instruments, Inc., private communication.

30. J. W. Allen et al, Appl. Phys. Lett., 7, 1965, p. 78.

31. C. Kittel, Introduction to Solid State Physics, 2d ed., John Wiley & Sons, New York, 1961, p. 154.

32. G. L. Pearson and F. Vogel, Progress in Semiconductors, 6, Heywood and Company, London, 1962, p. 3.

33. M. Gershenzon and R. M. Mikulyak, J. Appl. Phys., 35, 1964, p. 2132.

34. W. B. Daniels, Conf. on Semicond. Phys., Exeter, England, 1962, p. 482.

35. H. Fritzsche and J. J. Teimann, Conf. on Semicond. Phys., Dunod, France, 1964, p. 599.

36. G. Picus et al, J. Phys. Chem. Solids, 8, 1959, p. 282.